Formation of Metal in the CH Chondrites ALH 85085 and PCA 91467

ANDREW J. CAMPBELL* AND MUNIR HUMAYUN

Department of the Geophysical Sciences,
The University of Chicago, Chicago, Illinois 60637 USA
*email: a-campbell@uchicago.edu
ph: (773) 834-1523, fax: (773) 702-9505

In Press: Submitted to *Geochim. Cosmochim. Acta* July 3, 2003; accepted November 11, 2003

Abstract–Siderophile element distributions within individual metal grains in two CH chondrites, Allan Hills 85085 and Pecora Escarpment 91467, were measured by laser ablation inductively coupled plasma mass spectrometry. Those metal grains that are zoned in Ni were also found to be zoned in other refractory siderophile elements, such as Ru, but not in Pd, which is not refractory but is highly siderophile. This pattern is consistent with an origin by condensation from a gas of approximately solar composition, but not with an origin by redox processes or fractional crystallization. The unzoned metal grains in CH chondrites were found to be frequently depleted in Ru but not in Pd, consistent with later stage condensation from a solar gas after removal of the zoned metal. Gold is inversely correlated with Ni in the unzoned metal grains, and mean Au abundances in zoned metal are always low. Both zoned and unzoned metal in CH chondrites could plausibly be produced from a thermostatically regulated nebula, followed by rapid removal of the zoned metal, and slower removal of the unzoned metal, both at temperatures near or above the condensation temperature of Au (~1250 K). This is also consistent with the isolation temperatures inferred from silicate grains in CH chondrites by previous workers based on their volatile element inventories. The volatile siderophile Cu is enriched in the rims relative to the interiors of both zoned and unzoned grains, and is interpreted as the product of diffusion during low-grade thermal processing. The similarity of Cu distributions, and degree of kamacite/taenite exsolution, between zoned and unzoned metal in CH chondrites suggests that the two populations of metal experienced modest thermal metamorphism after they were brought together in the same environment, probably on the CH parent body. Fragmentation and size-sorting of the metal must have post-dated the Cu zoning, and may have occurred in a regolith on the CH parent body. The compositions of CH metal, like that of metal from QUE 94411 and HH 237, are consistent with a nebular origin, and may be the most primitive nebular materials (as distinct from presolar grains) sampled by chondrites.

1. INTRODUCTION

Primitive chondrites record the conditions and processes that occurred in the solar nebula during the early stages of solar system evolution. Examination of these meteorites and their components can potentially provide information on the range of temperatures and compositions present in the nebula at that time, as well as the timescales over which these conditions changed. Gas-solid exchange, in the form of volatilization and condensation, is known to be an important process in this evolution. For example, the compositions of the oldest solid solar system components, Ca-Al-rich inclusions (Amelin et al., 2002), are understood as high-temperature mineralogical assemblages, relative to the magnesian silicates that dominate chondrite compositions (Grossman, 1972; 1980; Grossman et al., 2000). The thermal structure of the protoplanetary disk, or solar nebula, was governed by the mass accretion rate and the disk optical depth (e.g. Humayun and Cassen, 2000), and the midplane temperatures in the inner disk at times of high mass accretion rate were thermostatically regulated by the condensation temperatures of the most abundant mineral components, particularly forsterite and Fe-Ni metal (Morfill, 1988; Boss, 1998; Cassen, 2001). The metal in primitive chondrites is believed to hold a chemical record of processes in the inner solar nebula (e.g. Meibom et al., 2000; Campbell et al., 2001). Thus, interpreting the conditions under which metal formed is fundamental to our understanding of the early solar system.

Most metal in chondrites, however, is the end-product of chondrule formation overprinted by metamorphism (Wood, 1967; Humayun and Campbell, 2002). Recently, a set of chondrite

types, the "CR clan," has been identified in which the bulk compositions are generally volatile-depleted, and the metamorphism of the rocks is greatly reduced (Weisberg et al., 1995; Krot et al., 2002), indicating that these meteorite groups, including the CR (Weisberg et al., 1993), CH (Bischoff et al., 1993), CB_a, and CB_b (Weisberg et al., 2001) chondrites, offer excellent opportunity for study of the high temperature processes related to the formation of the chondrite components prior to parent body accretion. These meteorites are generally metal-rich, and it was recognized early that the chondritic Co/Ni ratios that are commonly observed in their metal grains are not only a testament to the low degree of metamorphism experienced by the metal, but also a clue to its nebular formation (Wood, 1967; Grossman and Olsen, 1974; Weisberg et al., 1988).

Grossman and Olsen (1974) noted that Ni and Co in metal from C2 chondrites are positively correlated on the calculated path of equilibrium condensation from the solar nebula. Newsom and Drake (1979) observed such a correlation in metal in the Bencubbin (CB_a) meteorite, with an approximately chondritic Ni/Co ratio, and suggested that this metal was the product of nebular condensation. Weisberg et al. (1988; 1993) made similar interpretations of grain-to-grain variations in CR chondrites and in Allan Hills (ALH) 85085 (CH). Meibom et al. (1999) and Weisberg et al. (1999) noted that the range of compositions of P, Si, Cr, Co and Ni within individual zoned metal grains in CH and CB_b chondrites generally followed calculated condensation paths. If these grains did form by condensation, then the compositional zoning recorded in them may be used to constrain the cooling rate and oxidation state of the gas from which they grew (Meibom et al., 1999; 2000; 2001; Campbell et al., 2001; Petaev et al., 2001; 2003). Campbell et al. (2001) used trace siderophile element analyses to verify that the zoned metal grains in the CB_b chondrite Queen Alexandra Range (QUE) 94411 were indeed the products of condensation, and furthermore, that the PGE distributions were not consistent with simple fractional condensation but perhaps with non-equilibrium condensation from a gas supersaturated with siderophiles. In contrast, similar analyses demonstrated that nebular condensation was not responsible for the metal compositions in Bencubbin (Campbell et al., 2002a) or in Grosvenor Mountains (GRO) 95551 (Campbell and Humayun, 2003a), an ungrouped chondrite with many features similar to the CB_a chondrites (Weisberg et al., 2001).

Not all workers accept a nebular condensation origin of these meteorites, or of chondritic metal with solar Ni/Co ratios. Wasson and Kallemeyn (1990) argued that ALH 85085 (CH) formed by condensation from an impact-generated vapor cloud, and that the high metal-silicate ratios were the result of regolithic processes. Campbell et al. (2002a) showed that the siderophile element characteristics of metal in the CB_a chondrites, Bencubbin, Gujba and Weatherford, were not produced by condensation from the canonical solar nebula (P~10 Pa), and concluded that these metals may have formed by condensation from an impact-generated vapor plume. Metal compositions in Renazzo (CR) appear to have formed by a volatilization/recondensation process that is connected to chondrule processing (Connolly et al., 2001; Humayun et al., 2002; Zanda et al., 2002). Thus, a nebular origin of each of these chondrite types needs to be established before robust conclusions regarding astrophysical processes in the solar nebula can be reached.

To extend our understanding of the formation of these meteorites, and to investigate the relationship between the zoned and unzoned metal in CH chondrites, we have measured the distribution of siderophile elements in metal in Pecora Escarpment (PCA) 91467 and ALH 85085 by laser ablation ICP-MS (LA-ICP-MS). Arguments for or against the origins of the coarse (>40 μm) metal fraction of CH chondrites by nebular condensation, condensation from impact plumes, formation by chondrule processing, etc., are presented, and the possible astrophysical implications are discussed. Preliminary results of this study were reported by Campbell and Humayun (2002; 2003b).

2. EXPERIMENTAL

Polished thin sections of ALH 85085 and PCA 91467 were obtained from the United States Antarctic Meteorite Collection. The specimens were examined optically and studied using a JEOL 5800LV scanning electron microscope (SEM) with an Oxford Link/ISIS EDX system. The metal grain sizes in CH chondrites are relatively small, and range up to ~200 μm in the sections studied. Compositional profiles across

many of the largest (>100 μm) metal grains in the sections were determined by EDX; these revealed whether or not a particular grain was of the zoned or unzoned variety, and allowed an estimate of the degree of kamacite/taenite exsolution that had occurred in each grain. On the basis of this information, individual metal grains were selected for siderophile element analysis by LA-ICP-MS.

The laser ablation system utilized a CETAC LSX-200 laser ablation peripheral with a Finnigan MAT Element ICP mass spectrometer (Campbell and Humayun, 1999a,b; Campbell et al., 2002a; 2003). The standard 5x objective lens in the LSX-200 has been changed to a 10x lens, providing greater power density and sensitivity (Campbell et al., 2003). Argon gas is used to carry the ablated material through tygon tubing from the sample chamber of the LSX-200, to a 50 ml Savillex spray chamber, and then to the ICP. The purpose of the spray chamber is to extend the duration over which the laser-ablated material is measured by the ICP-MS. With no spray chamber a transient signal from the LSX-200 passes through the ICP-MS in ~10 s (Campbell and Humayun, 1999a), but the 50 ml spray chamber spreads the signal over ~20 s, which we have found to be a satisfactory compromise between signal longevity and minimization of accumulated background.

Because of the relatively small size of metal grains, the analyses were optimized for high spatial resolution by reducing the laser spot size to 13 μm diameter (~10 μm depth) and restricting the number of isotopes that were analyzed. Most of the LA-ICP-MS analyses measured ^{57}Fe, ^{59}Co, ^{60}Ni, ^{63}Cu, ^{101}Ru, and ^{105}Pd. The trace elements Cu, Pd, and Ru were chosen to represent a range of volatilities relative to that of Fe (Cu>Pd≈Fe>Ru), and Fe and Ni were required as major elements in the target material. A separate set of LA-ICP-MS analyses instead measured ^{53}Cr, ^{57}Fe, ^{60}Ni, ^{193}Ir, and ^{197}Au; in this case Ir was the representative refractory siderophile and Au was the representative volatile siderophile. Each analyzed point was ablated by 20 laser pulses at 10 Hz. The mass spectrometer was swept repeatedly over the intended mass range while the ablated material was carried by Ar gas from the sample chamber to the mass spectrometer. The signal from the transient laser ablation pulse was integrated over a period of ~20 s; this was sufficient time for the pulse to reach a peak intensity and then decay almost to background levels. Blank subtractions (average of 3 measurements with the laser off) were made, and an interference correction for ^{40}Ar^{61}Ni on ^{101}Ru was also done, although this was negligible. Instrumental sensitivity factors for each isotope were determined by measuring signal intensity from the group IIA iron meteorite Filomena and the NIST reference steel SRM 1263a, which have known concentrations of the elements of interest (Wasson et al., 1989; Campbell and Humayun, 1999b; Campbell et al., 2002a). The intensity data for each analysis were blank-subtracted and then corrected for the instrumental sensitivity factors. Laser ablation ICP-MS requires an internal calibrant. In the present case, because it is known that the target is a ferrous alloy, the internal calibrant was the sum of major elements Fe, Ni, and Co; in other words, the corrected intensity data were normalized to [Fe]+[Co]+[Ni]=100%. Previous comparison between several standards (Campbell et al., 2002a) has shown the reliability of this method. Detection limits for each analysis were based on the 3σ standard deviation of the three blank measurements.

Uncertainties of the LA-ICP-MS analyses reflect contributions from counting statistics as well as an instrumental error that is largely due to the transience of the signal. The counting errors incorporate both the measured counts and the counts in the blank measurement. The instrumental error was calculated from repeat measurements of the standards, by stripping away the counting errors from the variance of the standard analyses. This is a conservative estimate of the instrumental error because it assumes homogeneity in the standards, which are known to have fine scale heterogeneities. Instrumental errors (1σ) were assigned as 7.6%; this is the average value from several different calibrations.

3. RESULTS

3.1 Petrography

The section PCA 91467,25 is approximately 16 mm x 7 mm in size, and along one edge of it there is a fusion crust, ~1 mm thick, from which data were not obtained (Figure EA1). Section ALH 85085,9 is approximately 9 mm x 6 mm and has no unusual features specific to this section (Figure EA2). This section was described previously by Scott (1988), Weisberg et al.

(1988) and Wasson and Kallemeyn (1990). Both specimens are typical of CH chondrites (Scott, 1988; Weisberg et al., 1988; Grossman et al., 1988; Bischoff et al., 1993; 1994). Metal grains typically range in size from a few μm to ~200 μm (Figure 1). Chondrule metal is rare and smaller (≤5 μm), limiting the possibility of LA-ICP-MS analysis, and only isolated metal grains were analyzed here. Sulfides are rare in CH chondrites and commonly occur as μm-sized inclusions within metal (Weisberg et al., 1988; Grossman et al., 1988). Chondrules and silicate clasts, both having barred olivine, cryptocrystalline, and porphyritic textures in roughly equal proportions, have a similar size distribution to the metal. Glass is present in some chondrules.

Figure 2 shows Ni profiles across four different metal grains in ALH 85085, measured by SEM/EDX. Each profile is representative of a type that is common among the larger grains in CH chondrites. Figure 2a shows a zoned metal grain, with high Ni concentration in the core, reaching 12 wt%, decreasing toward the rim to ~4 wt%. The grain in Figure 2b shows no such zoning, but has a uniform Ni content of 5.7 wt%. Neither of the profiles in Figures 2a and 2b bear any evidence for subsolidus exsolution of kamacite from taenite. In contrast, Figures 2c and 2d show a zoned and unzoned grain, respectively, whose Ni profiles have been significantly disturbed by a plessitic decomposition into small, coexisting kamacite and taenite domains. The presence of plessite was documented earlier by Scott (1988) in the same section. Meibom et al. (1999) documented a similar range of Ni distributions in CH metal as observed in the present study and demonstrated the effect that kamacite/taenite exsolution had on interelement correlations such as the Ni-Co relationship, which is positively correlated in unexsolved grains but negatively correlated in extensively exsolved grains.

The metal grains chosen for further study by LA-ICP-MS were on the large end of the size range in these meteorites (~100 to 200 μm), had mostly subrounded shapes, and exhibited smooth Ni profiles, indicating minimal plessitic decomposition (Figure 1). Some of the grains contained small silicate inclusions, and a few (#PU3, PU4, PU5, PU7) contained a small number of fine (few μm) sulfide inclusions as well. Two unzoned grains, #AU3 and PU6, had narrow (few μm) silicate veins in them.

3.2 LA-ICP-MS Analyses of Zoned Metal Grains

LA-ICP-MS analyses of major- and trace-element distributions in a few typical zoned metal grains in PCA 91467 and ALH 85085 are presented in Table EA3, and some of these profiles are displayed graphically in Figure 3. As seen in Figure 3a, Ru is zoned in a similar fashion to Ni in these grains, with elevated Ru abundances reaching up to 12 ppm in the cores and diminishing to ~4 ppm at the rims. In contrast, Pd shows no such zoning but is instead homogeneously distributed throughout the same grains (Figure 3b). Copper abundances are typically uniform and low throughout the grain interiors, but rise sharply over the outermost 20-40 μm toward the rims, where they commonly reach ~100 ppm (Figure 3c). Likewise, Au is below the analytical detection limit in the grain interiors, and appears slightly elevated, at 0.2 to 0.4 ppm, at the rims of the zoned metal (Figure 3d). Even the highest Cu and Au concentrations measured in the rims of zoned metal remain subchondritic, with Cu/Fe and Au/Fe values <0.6x the CI value (Anders and Grevesse, 1989). Chromium also tends to be depleted in the grain cores more than at the rims, but the absolute chromium abundance is significantly different between the two zoned grains in which it was measured (Table EA3).

Data from a larger sampling of 5 zoned grains in ALH 85085 and 6 zoned grains in PCA 91467 are summarized in Figures 4a and 4b, which show the variations of Ru and Pd with Ni content. It is seen that Ru is positively correlated with Ni, but Pd shows no correlation with Ni. In the 2 zoned grains in which Ir and Au were measured, Ir is weakly correlated with Ni, like Ru, but Au is above detection limits only at the edge of the grains, where Ni is lowest, suggesting a negative correlation (Figures 4c and 4d). The range of Cu compositions is particularly large, and no single Cu-Ni trend is followed by all of the grains. However, within a single PCA 91467 grain (#PZ5), a negative Cu-Ni correlation is seen (Figure 5).

3.3 LA-ICP-MS Analyses of Unzoned Metal Grains

LA-ICP-MS data from unzoned grains are presented in Table EA4, and profiles from typical

unzoned grains are shown in Figures 3d and 6. Just as was observed in the Ni distributions, Ru, Pd, and Au show no systematic zoning in these grains within the analytical error. However, Cu contents rise steeply at the edges of unzoned grains, in a similar fashion to the Cu distribution in zoned grains (Figure 3c). The maximum value of Cu at the grain rims in unzoned grains (~100 ppm) is comparable to that observed in zoned grains, and the depth of penetration of Cu (~20-40 μm) is also similar in the two grain types. A single ~130 μm ALH 85085 grain (#AU3) exhibits high Cu abundances (287±23 ppm) throughout. No systematic difference was noted between those grains with small silicate and/or sulfide inclusions and those without. Furthermore, the presence of inclusions or veins had no detectable impact on the LA-ICP-MS profiles, indicating that they do not strongly affect the siderophile element budget, at least on the 15 μm length scale of the laser ablation analysis.

Mean compositions of the unzoned metal grains were calculated by summing the LA-ICP-MS signals from the individual spot analyses, and these results are included in Table EA4. A comparison between mean compositions of unzoned grains and the compositions within zoned metal (shown as individual analyses) is made in Figure 4. Figure 4a shows that, unlike the measurements of zoned grains, in which Ru is frequently enriched and correlated with Ni, the Ru contents in unzoned grains are not well correlated with Ni. Furthermore, the Ru contents of unzoned metal are frequently depleted relative to chondritic abundances and to the zoned metal. Mean Pd contents of unzoned metal, however, are similar to those in zoned metal, with approximately chondritic Pd/Fe values (Figure 4b). There is a negative correlation between Au and Ni in unzoned metal, with low (<0.1 ppm) Au contents at high Ni values, increasing to ~0.4 ppm Au at low Ni values (Figure 4d). A negative correlation also exists between Cr and Ni, and the range of Cr contents in the unzoned grains is greater than that seen in the zoned grains.

4. DISCUSSION

4.1 Possible Origins of Chondritic Metal

Metal in chondrites may originate by one of the following processes:

i) by condensation from a gas of solar composition, formed by evaporation of most or all pre-existing solids in the inner nebula, followed by grain formation during nebular cooling;
ii) from oxidized chondrule precursors by reduction of oxidized Fe from silicates, or desulfidation of FeNi-sulfides, during chondrule formation, followed by expulsion of metal from chondrules to form isolated grains;
iii) recondensation of Fe vapor volatilized from chondrules;
iv) condensation from vapor plumes formed by impact between chondritic and/or metallic asteroids.

The earliest attempts to explain the origin of chondrite metal assumed that Fe-Ni metal formed by condensation from the hot gas of the solar nebula (Wood, 1967; Grossman and Olsen, 1974). It was also recognized that most of the metal preserved in chondrites (mainly ordinary chondrites) had undergone metamorphism and exsolved into kamacite-taenite mixtures during cooling (Wood, 1967). Both Wood (1967) and Grossman and Olsen (1974) recognized the importance of metal from Renazzo and Al Rais (both CR chondrites) which had high Ni, but remained single-phase metal due to rapid cooling. Grossman and Olsen (1974) showed that the composition (Si, Cr, Co, Ni) of this metal was consistent with that calculated to form by condensation from a gas of solar composition, particularly the chondritic Co/Ni ratio.

Many subsequent workers have followed this same line of reasoning for the origin of metal in CB, CH and CR chondrites (Newsom and Drake, 1979; Weisberg et al. 1988; Grossman et al., 1988; Meibom et al., 1999). However, the chondritic Co/Ni ratio is mostly an indication that kamacite-taenite exsolution has not occurred, which would result in a negative correlation of Co and Ni, and all the processes outlined above could generate metal with an initially chondritic Co/Ni ratio. Metal present in chondrules may be regarded to form via process (ii) (Connolly et al., 1994), but metal occurring isolated in the matrices of chondrites is not similarly constrained. Additional elemental information is required to constrain the origins of metal occurring in chondrite matrices, such as that in CH and CB chondrites.

The elements Fe, Co and Ni are rather similar in their condensation properties (T_c: Ni>Co>Fe) and their resistance to oxidation (Ni>Co>Fe). Some siderophile elements, including W, Re, Os, Ir, Pt, Mo, Ru and Rh, are significantly more refractory than Ni; Pd is about the same volatility as Fe; Au and Cu are more volatile than Fe (Palme and Wlotzka, 1976; Kelly and Larimer, 1977; Wai and Wasson, 1977; Campbell et al., 2001). Most of these elements are also more siderophile than Ni, with the exception of W and Mo (Fegley and Palme, 1985; Humayun and Campbell, 2002). Campbell et al. (2001) used LA-ICP-MS to obtain siderophile element abundances on zoned metal grains from QUE 94411, a CB_b chondrite, and showed from the chondritic Pd/Fe ratios that reduction processes were not involved, but that the grains must have formed by condensation from a gas of solar composition at pressures (10 Pa) compatible with the inner portion of nebular disks (Wood and Morfill, 1988). In these grains, the refractory elements Mo, Ru, Rh, W, Re, Os, Ir and Pt followed Ni and Co in their zoning patterns. Campbell et al. (2002a) extended this to the CB_a subgroup, mainly Bencubbin metal, which also exhibits chondritic Co/Ni ratios, and showed that Bencubbinite metal had distinct Pd/Fe ratios that were not compatible with either reduction processes or condensation from a gas of solar composition at pressures compatible with the nebular disk. Instead, condensation from a metal-enriched gas at pressures about a 1000-fold higher than nebular pressures provided an adequate fit to the data. This was interpreted as being compatible with condensation from an impact-generated vapor plume (Campbell et al., 2002a). Connolly et al. (2001) and Humayun et al. (2002) studied siderophile element distributions in metal in the Renazzo (CR) chondrite, where it occurs in chondrules, on chondrule rims and as isolated grains in the matrix. Renazzo metal also exhibits chondritic Co/Ni ratios (Weisberg et al., 1988, 1993), but siderophile elements, particularly Pd, indicate the role of reduction processes during chondrule formation, and recondensation of Fe, Pd, Au and Cu from the surrounding vapor on to chondrule rim metal. With the exception of the metal from QUE 94411 and Hammadah Al Hamra (HH) 237, both CB_b chondrites, none of the metal from CB_a or CR chondrites resembles zoned metal from ALH 85085 or PCA 91467 described in this study. However, chondrule rim metal from CR chondrites might be similar to unzoned metal grains from the CH chondrites. The specific origins of the two metal types observed in CH chondrites is discussed separately below.

4.2 Formation of Zoned Metal

The three original papers describing ALH 85085 each concluded that the metal and silicate fractions of ALH 85085 had formed by nebular processes (Grossman et al., 1988; Scott, 1988; Weisberg et al., 1988). Meibom et al. (1999) interpreted the zoning that is commonly seen in CH chondrites as the product of fractional condensation from a cooling gas. In their model, the grain core represents refractory-rich metal that condensed at high temperatures in the solar nebula, and condensation continued as the gas cooled, forming metal with progressively lower contents of refractory elements toward the rim. Meibom et al. (1999) drew this interpretation primarily on the basis of the Ni and Co zoning, and the approximately solar Ni/Co ratios that are observed in these metal grains. Additional support was provided by the Cr, P, and Si distributions, which showed concave downward zoning (lower contents in the core) that is consistent with the condensation model of Grossman and Olsen (1974). However, it is also the case that Cr, P, and Si are less siderophile than Fe, while Ni and Co are more siderophile. The analysis by Meibom et al. (1999) focussed on the relative volatilities of the elements but did not exclude the possibility that the elements were fractionated by redox processes instead of a volatility-controlled process such as condensation. Meibom et al. (1999) further demonstrated how later metamorphism produced variable degrees of kamacite/taenite exsolution in CH chondrite metal, destroying the zoning and solar Ni/Co ratios in some cases.

The present study permits a more stringent test of the chemical property that primarily governed the zoning patterns observed in CH metal. The platinum group elements (PGEs) Ru and Pd are both highly siderophile, and would fractionate from Fe equally in most redox processes, but differ significantly in their volatilities. Ruthenium is a highly refractory siderophile element, with a condensation temperature (T_c) of ~1560 K in a solar gas at 10 Pa total pressure, but Pd is similar in volatility to Fe (T_c ~1350 K). Therefore Ru and Pd are expected to fractionate from one another during

condensation or volatilization of metal, but not during redox processing; conversely, Pd and Fe will be fractionated by redox processes but not by volatilization/condensation.

Typical profiles of Ru and Pd in zoned metal grains in the CH chondrites (Figure 3) show clearly that Ru is zoned like Ni but Pd is not. The process responsible for Ru/Fe fractionation, and no Pd/Fe fractionation, must have been volatility-based and not redox-based, consistent with the conclusions of Meibom et al. (1999). The fact that the refractories are concentrated in the cores, and not the rim, of the grains implies a condensation, and not volatilization, origin for the metal. Thus, the origin of the zoned metal in ALH 85085 and PCA 91467 is similar to that of zoned metal grains from QUE 94411 and HH 237 (Campbell et al., 2001), despite the differences in grain size. Campbell et al. (2001) also eliminated the possibility that chemical signatures such as these could have been generated by fractional crystallization from a melt (Scott, 1972).

A more quantitative test of the proposed condensation origin for the zoned metal is presented in Figure 4. Here the Ru and Pd measurements made in 11 zoned grains are plotted against Ni and compared to the trajectory of compositions calculated for metal condensing from a gas of solar composition at 10 Pa total pressure, over the temperature range 1350 K to 1150 K. The calculations shown here are taken from Campbell et al. (2001), and are similar to earlier work (e.g., Wlotzka and Palme (1976), Kelly and Larimer (1977), Wai and Wasson (1977)). The positive correlation between the refractory siderophiles Ru and Ni is seen to agree with the condensation calculation; likewise, the flat Pd trend in Figure 4b is expected during condensation, because of the similarity between the condensation temperatures of Pd and Fe. Decreases in Ni content of metal are caused by the addition of Fe, with Pd in chondritic Pd/Fe ratios.

Campbell et al. (2001) described two models for growth of the zoned metal grain in QUE 94411 by gas-solid exchange (Figure 7) which are equally applicable to zoned metal from the CH chondrites studied here. The first invokes rapid condensation of metal from a cooling gas, during which each successive shell of metal deposited on the surface reflects a progressively lower condensation temperature. This model is similar to that described by Meibom et al. (1999) based on Ni, Co, and Cr profiles in CH metal, except that Campbell et al. (2001) required that the gas be supersaturated in refractory elements during cooling. Without such supersaturation, it was argued, one would expect fractional condensation to cause all of the highly refractory siderophiles to be concentrated in the innermost few microns of the grain, which is not observed. The other model described by Campbell et al. (2001) invoked a preexisting small grain, enriched in Ni and refractories, upon which a layer of Fe-rich metal was condensed, followed by a period of diffusional equilibration between the two layers to form the observed zoning (Figure 7).

Resolution between the two models is essential to an understanding of the environment in which the zoned metal formed. In the gradational condensation model, a mean cooling rate ($\Delta T/\Delta t$) of the gas can be calculated from the observed size and zoning profile (Meibom et al., 1999; 2000; Campbell et al., 2001); assuming a composition and pressure for the gas, ΔT is determined by comparison of the observed core and rim compositions with the calculated condensation trajectory, while Δt is determined from the growth rate of the grain as predicted by the kinetic theory of gases. Estimates of cooling rates determined in this way are a few K/day for a solar gas at 10 Pa, yielding cooling timescales of ~1-3 weeks (Meibom et al., 1999; 2000; Campbell et al., 2001). If the two-stage condensation+diffusion model is correct, however, then these estimates of cooling rate are invalidated because the timing of grain growth may be more complicated than the one-stage process assumed in the gradational condensation model. The two models are not mutually exclusive, and simultaneous condensation from a cooling gas and diffusion within the growing grain must have taken place (Campbell et al., 2001; Petaev et al., 2003). Petaev et al. (2003) have modelled simultaneous condensation and diffusion of Fe, Ni, Co, and Cr in CH metal grains; they find that the zoning profiles can be fit with a cooling rate that accelerates with decreasing temperature, and overall timescales of ~5-10 weeks.

One approach to better understanding the effects of diffusion of refractory siderophiles in the zoned grains is the accurate determination of the relative diffusion rates of these elements in Fe. Diffusion data for a few of the elements of interest do exist (Mehrer et al., 1990), but a significant difficulty has been that interlaboratory

comparisons of diffusion rates frequently show significant disparities, presumably due to differences in sample condition, data refinement methods, etc. Righter et al. (2003) have attempted to overcome this problem by measuring multiple elements simultaneously in each experiment, with trace element doping levels comparable to the natural abundances. Diffusivities obtained for Ir and Ru from their study imply diffusive relaxation timescales ($t \sim r^2/D$, where r is grain radius and D is diffusivity) of about 10 weeks.

The same may not be true for some volatile siderophile elements, however. Figure 3c shows the distribution of Cu in zoned metal grains in ALH 85085 and PCA 91467. The Cu content is typically on the order of 100 ppm at the rims of the grains, and decreases to a few ppm over a short distance into the grain, about 20 to 40 μm. A similar, but less extreme, pattern was seen in Au (Figure 3d). The abundance of Au in the zoned metal cores is below the detection limit (~0.09 ppm) under the present analytical conditions, but increases reaching 0.2 to 0.4 ppm at the rims. Although the Cu distributions are qualitatively similar to the expected behavior of a volatile element during zoned growth by condensation, in that they increase toward the grain rim, a detailed comparison between the data and the Cu-Ni condensation trajectory (Figure 5) shows that the match is not very good. Even on the logarithmic scale of Figure 5, the Cu is too high at positions interior to the rim.

Instead, we interpret the Cu-Ni pattern in Figure 5 as the result of diffusion of Cu inward from the rim. Because of the high volatility of Cu, very low concentrations are expected over nearly all of the grain interior, and even a small amount of diffusion will significantly disturb the Cu-Ni relationship from the condensation curve. Moreover, the diffusion coefficient of Cu is higher than that of Ni, so Cu can diffuse over the modest distances involved (20 to 40 μm) with less significant redistribution of Ni or the PGEs (Righter et al., 2003). A similar interpretation might be made for Au, but this is less certain because of the low abundances and associated large errors, even at the grain rims (Figure 3d). The source of Cu diffusing into the metal will be discussed further in Section 4.3 below. The low abundances of Cu and Au indicate a cut-off temperature between the T_c of Fe (~1340 K) and that of Au (~1280 K) for the isolation of the metal from the gas.

In the discussion above, it has been assumed that the zoned metal formed by condensation from a solar gas. Alternative origins, such as by reduction from chondrules, are not supported by the chondritic Pd/Fe ratios, and the zoning has not been observed in metal associated with chondrules in any other chondrite class. Wasson and Kallemeyn (1990) proposed that zoned metal may have formed by condensation from a vapor plume generated by impact on a body possibly of CR composition. Distinguishing condensation from an impact generated vapor plume of chondritic composition and the solar nebula is not simple, particularly as the P, T, X and fO_2 parameters of the vapor plume are likely to be variable and weakly constrained. Campbell et al. (2002a) showed that condensation at P>>10 Pa resulted in Pd becoming more refractory than Ni, so that Pd/Fe fractionation would be observed during condensation. Thus, condensation of CH chondrite metal from high pressure portions of a vapor plume can be excluded. However, the Wasson and Kallemeyn (1990) impact model cannot be ruled out on purely chemical grounds given the latitude available in chemical parameters required to rigorously test their model.

Such a model, in which the CH chondrites formed from the same material as other CR-clan meteorites, is not strictly excluded by the O and N isotope characteristics of CH chondrites. Their O isotope compositions are similar to those of other CR-clan chondrites (Clayton and Mayeda, 1999; Weisberg et al., 2001), and their $\delta^{15}N$ values are high, ~800‰, in the range of CB chondrites, ~200 to 1000‰ (Prombo and Clayton, 1985; Sugiura et al., 2000) but higher than CR chondrites,~190‰ (Kung and Clayton, 1978; Robert and Epstein, 1982) Sugiura and Zashu (2001) identified carbonaceous aggregates as the isotopically heavy N carriers in CH chondrites, and concluded that the $\delta^{15}N$ heterogeneity within these meteorites, as well as variations between ^{15}N-rich meteorite groups (including CR-clan members, ordinary chondrites, and CM2s), can be explained by subsequent heating and/or hydration which perturb the $\delta^{15}N$ values of the meteorite components toward the solar average.

A physical argument against the Wasson and Kallemeyn (1990) model is that in collisions between asteroidal bodies, the thermal energy of the vapor plume is always higher than the gravitational binding energy of the vapor to the body (e.g. Campbell et al., 2002a). This can be

described in terms of the thermal velocity of a gas molecule in the vapor plume at T=1350 K (~1000 m s^{-1}) as compared with its escape velocity from an asteroid, $18<v_{esc}<180$ m s^{-1} (for asteroids of 30<d<300 km). Thus, the products of condensation are not likely to be re-accreted to the same body, or even to a single body, making the formation of the CH and CB_b chondrites difficult to understand by this mechanism.

4.3 Formation of Unzoned Metal

Weisberg et al. (1988) showed that there is a positive correlation between Ni and Co among metal grains in ALH 85085, and that this is consistent with a condensation origin of the CH metal. In that study, no distinction was made between zoned and unzoned metal, and it is therefore unclear whether the Ni-Co correlation was driven solely by the zoned metal, or whether the unzoned grains also follow this trend. Furthermore, the genetic relationship (if any) between zoned and unzoned grains has not been carefully investigated. Figure 8 shows that, in unzoned grains that have not undergone extensive kamacite/taenite exsolution, the positive Ni-Co correlation persists. In this section we examine other siderophile element distributions within individual unzoned grains and among different unzoned grains, to better understand the formation of these grains as well as the zoned metal.

Profiles of Ru, Pd, and Au reveal no significant zoning in the unzoned metal (Figures 3d and 6). Mean Ru, Pd, Ir, and Au abundances in the unzoned metal grains are plotted against Ni in Figure 4, where they are directly compared to the compositions measured within zoned metal. The Pd compositions in the unzoned metal, like those in zoned metal, cluster around chondritic abundances and show little fractionation from Fe, indicating Pd/Fe fractionating processes such as oxidation and subsolidus exsolution have had little impact on this metal. However, important distinctions between the unzoned and zoned metal can be observed in their refractory (Ru, Ir) and volatile (Au) siderophile element contents.

First, Ru is sometimes depleted in the unzoned metal relative to that expected from condensation from a gas of solar composition (Figure 4a). For example, the Ni content of unzoned metal grain #AU1 (7.3 wt%), if it were in equilibrium with a gas of solar composition, would imply 5.2 ppm of Ru – 4.5x higher than the observed value. The metal compositions observed in the unzoned grains can only have formed by condensation if it occurred in a gas that had been previously depleted in refractory siderophiles. In contrast, the data from zoned metal commonly shows Ru enrichments relative to chondritic abundances, and never exhibits strong Ru depletions (Figure 4a). Iridium, which like Ru is highly refractory, exhibits similar behavior in the unzoned metal; some of the Ir contents plot along the calculated condensation trajectory while others lie below it (Figure 4c).

Second, the Au abundances in unzoned metal are frequently greater than even the highest values in zoned metal. At high Ni contents, the Au is low in unzoned metal, but below ~7 wt% Ni the Au increases sharply (Figure 4d). This trend is in general agreement with the condensation trajectory calculated for a gas of solar composition at 10 Pa, which was taken from Campbell et al. (2001; 2002a). It bears noting that the high-temperature (high-Ni) portion of this calculation is sensitive to the activity coefficients used for Au dissolved in Fe-Ni alloy, which are poorly constrained. Campbell et al. (2001; 2002a) assumed ideal solid solution; activity coefficients higher (lower) than 1.0 would generate correspondingly lower (higher) Au contents in the condensed metal. (The calculations are not very sensitive to the activity coefficients of the refractory PGEs over the temperature range of Fe-Ni condensation, precisely because of their refractory nature.)

Reisener et al. (2000) proposed that unzoned grains may have formed from zoned grains by homogenization. Such an interpretation is fit by only a few grains, including #AU4, which plot on the same trends as zoned metal grains. Other grains require a different interpretation. Metal grains depleted in refractory siderophiles occur in the Renazzo chondrite, particularly as rim metal (Connolly et al., 2001; Humayun et al., 2002; Zanda et al., 2002; Campbell et al., 2002b). The origin of this metal is inferred to be condensation of Fe, Pd, Au and Cu from gas formed by evaporation of chondrules on to nuclei of refractory Ni-rich metal. The extent of recondensation can be large enough to form grains with subchondritic Ni/Fe and Ru/Fe ratios (Humayun et al., 2002). Although it cannot be ruled out that unzoned metal of refractory-depleted composition was formed this way in the CH chondrites, there exists a complementary relation between zoned metal, which is enriched in Ni and

refractory siderophile elements, and unzoned metal, which is usually depleted in these elements. Thus, unzoned metal and zoned metal were probably formed by the same process, condensation from a gas of solar composition, but the unzoned metal formed after the gas became depleted in refractory constituents. This depletion would have occurred in part because of the growth of the zoned metal; however, the highly refractory elements Ru and Ir are, in general, depleted in the unzoned grains more than Ni is, yet they are not enriched more than Ni in the zoned grain cores. Therefore it is possible that an additional mechanism of refractory metal depletion also affected the gas from which the unzoned grains formed. It is evident that zoned metal formed by gas-solid exchange to record μm-scale zoning, whereas the unzoned metal could have formed by diffusive equilibration of solids that were not isolated as rapidly from the gas as zoned metal was.

4.4 Late-stage Processing of CH metal

To preserve the distinct refractory-rich, volatile-poor chemical compositions of both zoned and unzoned metal grains in CH chondrites, rapid isolation from the cooling gas is required at T~1340-1280 K at 10 Pa. Unlike the distribution of most siderophile elements (e.g., Ni, Ru, Pd, Ir, Au described above), Cu is enriched at the rims of the unzoned metal grains, relative to their cores, in a manner very similar to that of the Cu distribution in zoned metal (Figures 3c and 6). Copper abundances are typically ~100 ppm at the rim of unzoned metal, decreasing over a distance of 20-40 μm to a few ppm in the grain interiors. The similarity of the Cu distributions within unzoned grains (Figure 6) and zoned grains (Figure 3c) suggests that the Cu enrichments at the rims of the two metal populations may have a common origin.

It was concluded above that Cu diffused into the zoned metal grains from the rims subsequent to the formation of the grain and its zoning pattern, and that the zoned and unzoned metal grains formed at different stages of the condensation process. Therefore, it is likely that Cu diffused into both metal grain populations simultaneously, after they had been brought together in a common environment, probably the CH parent body. Moreover, the unzoned metal and zoned metal have been subjected to similar degrees of kamacite/taenite partitioning (Figure 2; Meibom et al., 1999). It is therefore likely that minor Cu diffusion into the rims and incipient kamacite/taenite exsolution that are observed in CH metal both occurred during modest thermal metamorphism after accretion onto the CH parent body. It is not necessary that this metamorphism occurred in the present state of assembly of the meteorite; a significant degree of regolith mixing may have subsequently occurred on the parent body, as suggested by the presence of hydrous matrix lumps in CH chondrites (Grossman et al., 1988; Scott, 1988; Weisberg et al., 1988; Greshake et al., 2002).

An alternative hypothesis is that Cu diffused into the metal while it still resided in the nebula. In this model Cu would begin to be deposited onto the metal surface when the gas cooled to ~1170 K (at 10 Pa), and it would then diffuse inward more rapidly than Ni and other siderophiles could equilibrate, given its higher diffusivity (Mehrer, 1990; Righter et al., 2003). However, the diffusion of Cu would quickly raise the surface Cu contents to much higher values (600 ppm) than observed, requiring very brief exposure to the nebula at T<1170 K. This scenario would require that zoned and unzoned grains experience similar nebular histories in this temperature range, despite having different histories at higher temperature.

In our preferred model of parent-body diffusion, the Cu source could be any minor volatile-rich component in the parent body, which could include, for example, fine-grained metal and sulfide or even the fine-grained "dark inclusions" or "hydrated lithic clasts" described in detail by Weisberg et al. (1988), Grossman et al. (1988), and Greshake et al. (2002). Because of the fine-grained nature of CH chondrites, grain boundary diffusion could allow rapid transport from the source to the metal grain surfaces. Tests of this scenario could include examination of possible Cu sources and their distribution. Furthermore, a similar distribution of rapid-diffusing, volatile lithophiles (e.g. Na, K) should be found at low abundances in the rims of silicate components in the meteorites, similar to that described by Grossman et al. (2002) from the LL3.0 chondrite Semarkona.

4.5 A Scenario for the Nebular Origin of CH metal

The following observations support a plausible nebular origin of the CH metal: metal

formed as a by-product of chondrule formation does not include zoned metal observed in CH and CB_b chondrites, and the zoned and unzoned metal appear to be complementary in siderophile element abundances. The more refractory behavior of Pd relative to Fe, Co and Ni, described by Campbell et al. (2002) for metal formed by condensation from high pressure vapor plumes and reported by these workers from Bencubbinite metal of the CB_a class is not present in the CH metal. Thus, an impact origin, while not fully ruled out by the chemical evidence, is also not supported. An origin by condensation from a gas of solar composition at pressures compatible with nebular pressures is indicated as the origin of the zoned metal. A scenario is proposed here that examines the consequences of origin by condensation of CH metal from a hot solar nebula.

At high mass accretion rates, mid-plane temperatures in the inner disk become sufficiently hot to completely vaporize most of the dust (e.g. Boss, 1998; Humayun and Cassen, 2000). The lowering of opacity by evaporation of the major dust components, particularly Fe-Ni metal, results in rapid cooling of the nebular gas to the condensation temperature of Fe-Ni metal, at which temperature the gas is thermostatically regulated (Morfill, 1988; Boss, 1998; Cassen, 2001). Transient heating events by shocks, clumpy accretion of interstellar gas, or other processes, will result in rapid evaporation of Fe-Ni metal, followed by rapid cooling as shown schematically in Figure 9.

Condensation of Fe-Ni metal following transient heating events is a plausible means of forming the zoned metal found in CH chondrites. To preserve such grains, rapid removal ($t < 5$ weeks) from the hot portion of the disk is required, similar to that proposed by Meibom et al. (2000) (the modelling of Petaev et al. (2003) suggests removal on a 5-10 week time scale). Metal that is subsequently melted, or remains in contact with the gas sufficiently long to diffusively equilibrate ($t >10$ weeks), will form unzoned metal. Some zoned metal may also be converted to unzoned metal by remaining at temperatures close to the T_c of metal for periods > 10 weeks. Rapid removal of refractory metal, including the zoned grains, will leave the residual nebular gas depleted in Ru, Ir and other refractory siderophiles. Metal which remains in the gas will continue to chemically exchange with this gas and acquire additional Fe and Pd, resulting in subchondritic Ir/Fe and Ru/Fe ratios while maintaining chondritic Pd/Fe ratios. The isolation temperatures for the metal are constrained by Ni/Fe and Au/Fe ratios to be ~1280-1350 K at 10 Pa nebular pressure. The degree of Ru and Ir depletion in unzoned metal is greater than that of Ni (Figure 4), and suggests, in some cases, the removal of metal that is even more refractory than the observed zoned metal. There is substantial variability in the peak temperatures, removal temperatures, and timescales inferred from metal compositions and size of different zoned grains, and there is also overlap between the compositions, hence temperatures, recorded in the zoned and unzoned grains. These may result from variability between multiple heating/cooling events (Figure 9), as well as spatial and temporal variations in individual heating cycles and grain removal processes. A similar conclusion, regarding variability in source conditions for formation of zoned metal, was reached by Petaev et al. (2003). Sugiura and Zashu (2001) also appealed to transient, nebular heating events to cause heavy nitrogen, originating from carbon-silicate aggregates, to be dissolved into metallic grains in PCA 91467. The mechanism proposed by Sugiura and Zashu (2001) would work equally well in the scenario described here for formation of CH chondrite metal. The reduced nature of CH chondrite silicates and their similar grain size to CH chondrite metal lend support to a common origin of both metal and silicate (Krot et al., 2001). Grossman et al. (1988) inferred that the silicate fraction had been agglomerated at T~1000 K based on alkali element abundances, broadly consistent with the observations made here.

The Cu zoning around both zoned metal and unzoned metal grains could have occurred either in the nebular gas, or post-accretion on the parent body. The Cu zoning is absent on some grains altogether (#AZ3, #AZ4), and is present only on one side of the traverse in other grains (#AZ1, #PZ4), implying that metal fragmentation during impacts on the CH parent body post-dated the Cu zoning. The CH parent body experienced a regolith history that introduced solar wind noble gases (Eugster and Niedermann, 1990), matrix lumps, chondrule fragments, and ferroan silicate grains into the reduced, high temperature metal and silicate component that constitutes ~90% of CH chondrites (Grossman et al., 1988; Scott, 1988; Weisberg et al., 1988; Wasson and Kallemeyn, 1990).

The preservation of high temperature condensates from a gas of solar composition requires an incompletely understood mechanism for the rapid removal of such material from hot nebular gas. The requirement for such a mechanism is not limited to the CH chondrites; for example, the source material for some Ga and Ge depleted iron meteorites, such as Group IVA and IVB, is not represented among the major chondrite classes (but Scott (1988) noted that CH chondrites are plausible precursors). The pervasiveness of this material in the inner solar system is further implied by the volatile depleted composition of planetary compositions (e.g. Earth, Mars, Moon, Eucrite parent body), which cannot be understood exclusively by combinations of the nine major chondrite classes (Humayun and Clayton, 1995). Based on the absence of K isotope fractionation, Humayun and Clayton (1995) concluded that the volatile element depletions observed in planetary compositions were not consistent with volatilization of known chondritic material, which all have volatile element abundances significantly higher than planetary materials, but required that volatile-poor materials, such as high temperature condensates, must have been incorporated by objects forming in the inner solar system. Such material is not represented in the ordinary, carbonaceous and enstatite chondrites present in meteorite collections, but appears to constitute the major fraction of CH chondrites.

Arguably, CH chondrites are among the most primitive nebular materials available, and provide insights into high temperature nebular processes affecting metal and other major constituents of protoplanetary material. Humayun and Cassen (2000) showed that a nebular cooling model where cooling was generated by opacity reduction associated with accretion of dust into chondritic planetesimals could account for the moderately volatile element abundances of most of the known chondrite classes (CVs being the most depleted ones). The timescales for these processes are on the order of 10^3-10^4 years. These models do not produce moderately volatile element depletions greater than about 0.3-0.4xCI, and do not account for the moderately volatile element depletions observed in most planetary materials (Humayun and Cassen, 2000). A process that transports high temperature condensates from the inner nebula to outer, cooler regions would conceivably provide the required sequestration of solid condensates from the hot nebular regions in which they formed. Meibom et al. (2000) proposed to use large convective instabilities in the disk to loft condensates to high nebular altitudes, where turbulent diffusion could transport a portion of the solid material outwards in the disk. Such an event leaves little chemical imprint from which to understand the transport process. Thus, at the present time, it is not possible to better constrain the mechanism by which high temperature condensates were preserved, except to observe that such a mechanism is required for reasons other than an explanation of the metal compositions of CH and CB_b chondrites.

5. CONCLUSIONS

Zoned metal grains in the CH chondrites ALH 85085 and PCA 91467 are enriched in Ni and other refractory siderophile elements in their cores relative to their rims, but Pd is nearly unfractionated between cores and rims in these grains. These siderophile element trends are compatible with formation of the zoned metal by condensation, similar to the interpretations made previously by Campbell et al. (2001) for zoned metal in the CB_a chondrite QUE 94411. The observed zoning cannot have been produced by redox processing or fractional crystallization, both of which would produce siderophile element fractionations that are different than those observed, including fractionation of the Pd/Fe ratio. The origin of the zoned metal is consistent with an origin by condensation from a gas of solar composition at a pressure of 10 Pa, which implies a nebular setting. Preservation of the zoning requires gas-solid exchange, with rapid isolation ($t < 10$ weeks), prior to the complete condensation of all Pd and Fe in the gas.

The unzoned metal in CH chondrites is frequently depleted in highly refractory elements such as Ru or Ir relative to their Ni contents, in contrast to the zoned grains which generally have refractory-rich mean compositions. Likewise, mean abundances of the volatile element Au are frequently higher in unzoned grains than in zoned grains. These differences in mean composition between zoned and unzoned metal indicate that the unzoned metal is not simply a homogenized form of the zoned metal (although some grains may be formed in this manner), but may have formed at a later stage of the same process that produced the zoned grains. The isolation T,

>1280 K, and the removal timescale, >10 weeks, are constrained by the elemental data and siderophile element diffusivities. Both zoned and unzoned metal can plausibly be produced in a nebular process involving a thermostatically regulated nebula (T~1300 K) with transient heating events that vaporized the pre-existing Fe-Ni grains. A mechanism for the rapid removal of such grains remains to be established, but such a mechanism for transporting high temperature material processed in the inner nebula is required to explain the moderately volatile element abundances of planetary material. Metal from CH and CB_b chondrites are probably the most pristine major-element condensates sampled from the protoplanetary disk.

Copper enrichments at the metal rims, and strong depletions in the metal interiors, are observed in both zoned and unzoned metal in CH chondrites, but do not mirror the distributions expected on the basis of condensation calculations. These are interpreted as the products of minor re-equilibration during which rapidly diffusing Cu enters the outermost 20-40 μm of the metal without strongly affecting the distribution of most other siderophiles. The similarity in Cu distributions, and in minor degrees of kamacite exsolution, between zoned and unzoned metal suggests that these aspects of CH chondrite metal are products of minor, postaccretionary thermal processing. Assymetry in the Cu zoning in these metal grains further implies that metal fragmentation processes during brecciation in a regolith on the CH parent body postdated the Cu zoning.

Acknowledgments–We are grateful to the Meteorite Working Group for providing the sections of ALH 85085 and PCA 91467. The article benefitted from the comments of three anonymous reviewers and the associate editor, A. Krot. This work was supported by NASA through grants NAG5-9800 and NAG5-13133 to M. H.

REFERENCES

Amelin Y., Krot A. N., Hutcheon I. D., and Ulyanov A. A. (2002) Lead isotopic ages of chondrules and calcium-aluminum-rich inclusions. *Science* **297**, 1678-1683.

Anders E. and Grevesse N. (1989) Abundances of the elements: Meteoritic and solar. *Geochim. Cosmochim. Acta* **53**, 197-214.

Bischoff A., Palme H., Schultz L., Weber D., Weber H. W., and Spettel B. (1993) Acfer 182 and paired samples, an iron-rich carbonaceous chondrite: Similarities with ALH85085 and relationship to CR chondrites. *Geochim. Cosmochim. Acta* **57**, 2631-2648.

Bischoff A., Schirmeyer S., Palme H., Spettel B., and Weber D. (1994) Mineralogy and chemistry of the carbonaceous chondrite PCA 91467 (CH). *Meteorit. Planet. Sci.* **29**, 444.

Boss A. P. (1998) Temperatures in protoplanetary disks. *Annu. Rev. Earth Planet. Sci.* **26**, 53-80.

Campbell A. J. and Humayun M. (1999a) Trace element microanalysis in iron meteorites by laser ablation ICPMS. *Anal. Chem.* **71**, 939-946.

Campbell A. J. and Humayun M. (1999b) Microanalysis of platinum group elements in iron meteorites using laser ablation ICP-MS. *Lunar Planet. Sci. XXX*. Lunar Planet. Inst., Houston. #1974 (abstr.).

Campbell A. J. and Humayun M. (2002) Condensation of metal in a CH chondrite. *Meteorit. Planet. Sci.* **37**, A29.

Campbell A. J. and Humayun M. (2003a) Formation of metal in GRO 95551 and comparison to ordinary chondrites. *Geochim. Cosmochim. Acta* **67**, 2481-2495.

Campbell A. J. and Humayun M. (2003b) Zoned and unzoned metal grains in the CH chondrites ALH 85085 and PCA 91467. *Lunar Planet. Sci. XXXIV*. Lunar Planet. Inst., Houston. #1410 (abstr.).

Campbell A. J., Humayun M., and Weisberg M. K. (2000) Siderophile element distributions in zoned metal grains in Hammadah al Hamra 237. *Meteorit. Planet. Sci.* **35**, A38-A39.

Campbell A. J., Humayun M., Meibom A., Krot A. N., and Keil K. (2001) Origin of zoned metal grains in the QUE94411 chondrite. *Geochim. Cosmochim. Acta* **65**, 163-180.

Campbell A. J., Humayun M., and Weisberg M. K. (2002a) Siderophile element constraints on the formation of metal in the metal-rich chondrites Bencubbin, Weatherford, and Gujba. *Geochim. Cosmochim. Acta* **66**, 647-660.

Campbell A. J., Humayun M., and Zanda B. (2002b) Partial condensation of volatile elements in Renazzo chondrules. *Geochim. Cosmochim. Acta* **66**, A117 (abstr.).

Campbell A. J., Simon S. B., Humayun M. and Grossman L. (2003) Chemical evolution of metal in refractory inclusions in CV3 chondrites. *Geochim. Cosmochim. Acta* **67**, 3119-3134.

Cassen P. (2001) Nebular thermal evolution and the properties of primitive planetary materials. *Meteorit. Planet. Sci.* **36**, 671-700.

Clayton R. N. and Mayeda T. K. (1999) Oxygen isotope studies of carbonaceous chondrites. *Geochim. Cosmochim. Acta* **63**, 2089-2104.

Connolly H. C. Jr., Hewins R. H., Ash R. D., Zanda B., Lofgren G. E. and Bourot-Denise M. (1994) Carbon and the formation of reduced chondrules. *Nature* **371**, 136-139.

Connolly H. C. Jr., Huss G. R., and Wasserburg G. J. (2001) On the formation of Fe-Ni metal in Renazzo-like carbonaceous chondrites. *Geochim. Cosmochim. Acta* **65**, 4567-4588.

Eugster O and Niedermann S. (1990) Solar noble gases in the unique chondritic breccia Allan Hills 85085. *Earth Planet. Sci. Lett.* **101**, 139-147.

Fegley B. Jr. and Palme H. (1985) Evidence for oxidizing conditions in the solar nebula from Mo and W depletions in refractory inclusions in carbonaceous chondrites. *Earth Planet. Sci. Lett.* **72**, 311-326.

Greshake A., Krot A. N., Meibom A., Weisberg M. K., Zolensky M. E., and Keil K. (2002) Heavily-hydrated lithic clasts in CH chondrites and the related, metal-rich chondrites Queen Alexandra Range 94411 and Hammadah al Hamra 237. *Meteorit. Planet. Sci.* **37**, 281-293.

Grossman J. N., Rubin A. E., and MacPherson G. J. (1988) ALH85085: a unique volatile-poor carbonaceous chondrite with possible implications for nebular fractionation processes. *Earth Planet. Sci. Lett.* **91**, 33-54.

Grossman J. N., Alexander C. M. O'D., Wang J., and Brearley A. J. (2002) Zoned chondrules in Semarkona: Evidence for high- and low-temperature processing. *Meteorit. Planet. Sci.* **37**, 49-73.

Grossman L. (1972) Condensation in the primitive solar nebula. *Geochim. Cosmochim. Acta* **36**, 597-619.

Grossman L. (1980) Refractory inclusions in the Allende meteorite. *Ann. Rev. Earth Planet. Sci.* **8**, 559-608.

Grossman L. and Olsen E. (1974) Origin of the high-temperature fraction of C2 chondrites. *Geochim. Cosmochim. Acta* **38**, 173-187.

Grossman L., Ebel D. S., Simon S. B., Davis A. M., Richter F. M., and Parsad N. M. (2000) Major element chemical and isotopic compositions in refractory inclusions in C3 chondrites: The separate roles of condensation and evaporation. *Geochim. Cosmochim. Acta* **64**, 2879-2894.

Humayun M. and Campbell A. J. (2002) The duration of ordinary chondrite metamorphism inferred from tungsten microdistribution in metal. *Earth Planet. Sci. Lett.* **198**, 225-243.

Humayun M. and Cassen P. (2000) Processes determining the volatile abundances of the meteorites and terrestrial planets. In *Origin of the Earth and Moon* (eds. R. M. Canup and K. Righter). University of Arizona Press, Tucson, pp. 3-23.

Humayun M. and Clayton R. N. (1995) Potassium isotope cosmochemistry: Genetic implications of volatile element depletion. *Geochim. Cosmochim. Acta* **59**, 2131-2148.

Humayun M., Campbell A. J., Zanda B., and Bourot-Denise M. (2002) Formation of Renazzo chondrule metal inferred from siderophile elements. *Lunar Planet. Sci. XXXIII*. Lunar Planet. Inst., Houston. #1965 (abstr.).

Kelly W. R. and Larimer J. W. (1977) Chemical fractionations in meteorites – VIII. Iron meteorites and the cosmochemical history of the metal phase. *Geochim. Cosmochim. Acta* **41**, 93-111.

Krot A. N., Meibom A., Russell S. S., Alexander C. M. O'D., Jeffries T. E., and Keil K. (2001) A new astrophysical setting for chondrule formation. *Science* **291**, 1776-1779.

Krot A. N., Meibom A., Weisberg M. K., and Keil K. (2002) The CR chondrite clan: Implications for early solar system processes. *Meteorit. Planet. Sci.* **37**, 1451-1490.

Kung C. C. and Clayton R. N. (1978) Nitrogen abundances and isotopic compositions in stony meteorites. *Earth Planet. Sci. Lett.* **38**, 421-435.

Mehrer H. (1990) Diffusion in solid metals and alloys. In *Landolt-Börnstein Numerical Data and Functional Relationships in Science and Technology, Group III, Volume 26* (ed. O. Madelung). Springer-Verlag, Heidelberg.

Meibom A., Petaev M. I., Krot A. N., Wood J. A., and Keil K. (1999) Primitive FeNi metal grains in CH carbonaceous chondrites formed by condensation from a gas of solar composition. *J. Geophys. Res.* **104**, 22053-22059.

Meibom A., Desch S. J., Krot A. N., Cuzzi J. N., Petaev M. I., Wilson L., and Keil K. (2000) Large scale thermal events in the solar nebula recorded in Fe, Ni metal condensates in primitive meteorites. *Science* **288**, 839-841.

Meibom A., Petaev M. I., Krot A. N., Keil K., and Wood J. A. (2001) Growth mechanism and additional constraints on FeNi metal condensation in the solar nebula. *J. Geophys. Res.* **106**, 32797-32801.

Morfill G. E. (1988) Protoplanetary accretion disks with coagulation and evaporation. *Icarus* **75**, 371-379.

Newsom H. E. and Drake M. J. (1979) The origin of metal clasts in the Bencubbin meteorite breccia. *Geochim. Cosmochim. Acta* **43**, 689-707.

Petaev M. I., Meibom A., Krot A. N., Wood J. A., and Keil K. (2001) The condensation origin of zoned metal grains in Queen Alexandra Range 94411: Implications for the formation of the Bencubbin-like chondrites. *Meteorit. Planet. Sci.* **36**, 93-106.

Petaev M. I., Wood J. A., Meibom A., Krot A. N., and Keil K. (2003) The ZONMET thermodynamic and kinetic model of metal condensation. *Geochim. Cosmochim. Acta* **67**, 1737-1751.

Prombo C. A. and Clayton R. N. (1985) A striking isotope anomaly in the Bencubbin and Weatherford meteorites. *Science* **230**, 935-937.

Reisener R., Meibom A., Krot A. N., Goldstein J. I., and Keil K. (2000) Microstructure of condensate Fe-Ni metal particles in the CH chondrite PAT91546. *Lunar Planet. Sci. XXXI*. Lunar Planet. Inst., Houston. #1445 (abstr.).

Righter K., Campbell A. J., and Humayun M. (2003) Diffusion of siderophile elements in Fe metal: Application to zoned metal grains in chondrites. *Lunar Planet. Sci. XXXIV*. Lunar Planet. Inst., Houston. #1373 (abstr.).

Robert F. and Epstein S. (1982) The concentration and isotopic composition of hydrogen, carbon, and nitrogen in carbonaceous meteorites. *Geochim. Cosmochim. Acta* **46**, 81-95.

Scott E. R. D. (1972) Chemical fractionation in iron meteorites and its interpretation. *Geochim. Cosmochim. Acta* **36**, 1205-1236.

Scott E. R. D. (1988) A new kind of primitive chondrite, Allan Hills 85085. *Earth Planet. Sci. Lett.* **91**, 1-18.

Sugiura N. and Zashu S. (2001) Carbon-silicate aggregates in the CH chondrite Pecora Escarpment 91467: A carrier of heavy nitrogen of interstellar origin. *Meteorit. Planet. Sci.* **36**, 515-524.

Sugiura N., Zashu S., Weisberg M. K., and Prinz M. (2000) A nitrogen isotope study of bencubbinites. *Meteorit. Planet. Sci.* **35**, 987-996.

Wai C. M. and Wasson J. T. (1977) Nebular condensation of moderately volatile elements and their abundances in ordinary chondrites. *Earth Planet. Sci. Lett.* **36**, 1-13.

Wasson J. T. and Kallemeyn G. W. (1990) Allan Hills 85085: A subchondritic meteorite of mixed nebular and regolithic heritage. *Earth. Planet. Sci. Lett.* **101**, 148-161.

Wasson J. T., Ouyang X., Wang J. and Jerde E. (1989) Chemical classification of iron meteorites: XI. Multi-element studies of 38 new irons and the high abundance of ungrouped irons from Antarctica. *Geochim. Cosmochim. Acta* **53**, 735-744.

Weisberg M. K., Prinz M., and Nehru C. E. (1988) Petrology of ALH85085: a chondrite with unique characteristics. *Earth Planet. Sci. Lett.* **91**, 19-32.

Weisberg M. K., Prinz M., Clayton R. N., and Mayeda T. K. (1993) The CR (Renazzo-type) carbonaceous chondrite group and its implications. *Geochim. Cosmochim. Acta* **57**, 1567-1586.

Weisberg M. K., Prinz M., Clayton R. N., Mayeda T. K., Grady M. M., and Pillinger C. T. (1995) The CR chondrite clan. *Proc. NIPR Symp. Antarct. Meteorites* **8**, 11-32.

Weisberg M. K., Prinz M., Clayton R. N., Mayeda T. K., Sugiura N., Zashu S., and Ebihara M. (1999) QUE94411 and the origin of bencubbinites. *Lunar Planet. Sci. XXX*. Lunar Planet. Inst., Houston. #1416 (abstr.).

Weisberg M. K., Prinz M., Clayton R. N., Mayeda T. K., Sugiura N., Zashu S., and Ebihara M. (2001) A new metal-rich chondrite grouplet. *Meteorit. Planet. Sci.* **36**, 401-418.

Wood J. A. (1967) Chondrites: their metallic minerals, thermal histories and parent planets. *Icarus* **6**, 1-49.

Wood J. A. and Morfill G. E. (1988) A review of solar nebula models. In *Meteorites and the Early Solar System* (eds. J. F. Kerridge and M. S. Matthews). University of Arizona Press, Tucson, pp. 329-347.

Zanda B., Bourot-Denise M., Hewins R., Cohen B. A., Delaney J. S., Humayun M., and Campbell A. J. (2002) Accretion textures, iron evaporation and re-condensation in Renazzo chondrules. *Lunar Planet. Sci. XXXIII*. Lunar Planet. Inst., Houston. #1852 (abstr.).

FIGURE CAPTIONS

Figure 1. Ni K_α map of PCA 91467. Three types of Ni distribution in metal are indicated: zoned, unzoned, and having kamacite/taenite exsolution. The two large grains at the top have been analyzed by LA-ICP-MS. Scale bar = 200 μm.

Figure 2. Profiles of Ni content across typical metal grain types in ALH 85085, determined by SEM/EDX. a) Zoned metal with no kamacite/taenite exsolution; b) unzoned metal with no kamacite/taenite exsolution; c) zoned metal exhibiting kamacite/taenite exsolution; d) unzoned metal exhibiting kamacite/taenite exsolution. Trace siderophile analyses by LA-ICP-MS were performed principally on types a) and b), which are unaffected by subsolidus exsolution of the metal.

Figure 3. LA-ICP-MS measurements of a) Ru, b) Pd, c) Cu, and d) Au in zoned metal grains in ALH 85085 and PCA 91467. Each shade of symbol represents a different grain, as labelled in the legend. The detection limit of Au is indicated in d) by the dashed line. Profiles of unzoned grains are also included in d) for comparison.

Figure 4. Trace siderophile elements a) Ru, b) Pd, c) Ir, and d) Au vs. Ni data determined by LA-ICP-MS in metal grains from CH chondrites. Small open circles: values within several different zoned grains; large shaded circles: mean values for unzoned grains; short dashes: upper limits within zoned grains; long dashes: upper limits in unzoned grains; line: calculated condensation trajectory for a gas of solar composition at 10 Pa (Campbell et al., 2001).

Figure 5. Cu vs. Ni data determined by LA-ICP-MS in zoned metal grain #PZ5 in PCA 91467. Open triangles: Cu measurements in the grain; line: calculated condensation trajectory for a gas of solar composition at 10 Pa (Campbell et al., 2001).

Figure 6. LA-ICP-MS profiles across unzoned metal grain #AU4 in ALH 85085. Circles: Ru; squares: Pd; triangles: Cu; dashes: upper limits for Cu.

Figure 7. Schematic of two proposed models of formation of zoned metal grains (Campbell et al., 2001). In the first model, the compositional zoning within each grain reflects the change in composition of metal condensing from the gas as the temperature falls. In the second model, a refractory-rich core is overlain by metal that is not refractory, and subsolidus diffusion only partly equilibrates the two layers. The effect of either model is to form a zoned grain with a gradient in refractory enrichment from the core to the rim.

Figure 8. Co vs. Ni data determined by LA-ICP-MS in metal grains from CH chondrites. Open circles: Co values within several different zoned grains; shaded circles: mean Co values from unzoned grains; line: calculated condensation trajectory for a gas of solar composition at 10 Pa (Campbell et al., 2001).

Figure 9. Schematic illustration of the temperature-time path in a thermostatically regulated solar nebula showing how both zoned metal and unzoned metal from CH chondrites can form by the same process.

ELECTRONIC ANNEX

Figure EA1. Backscattered electron image of PCA 91467. The meteorite consists primarily of fine-grained silicate clasts, chondrules and metal. A fusion crust of ~1 mm thickness is visible along the top edge. Scale bar = 2 mm.

Figure EA2. Backscattered electron image of ALH 85085. The meteorite consists primarily of fine-grained silicate clasts, chondrules and metal. Scale bar = 2 mm.

Table EA3. LA-ICP-MS data from zoned metal grains.

Table EA4. LA-ICP-MS data from unzoned metal grains.

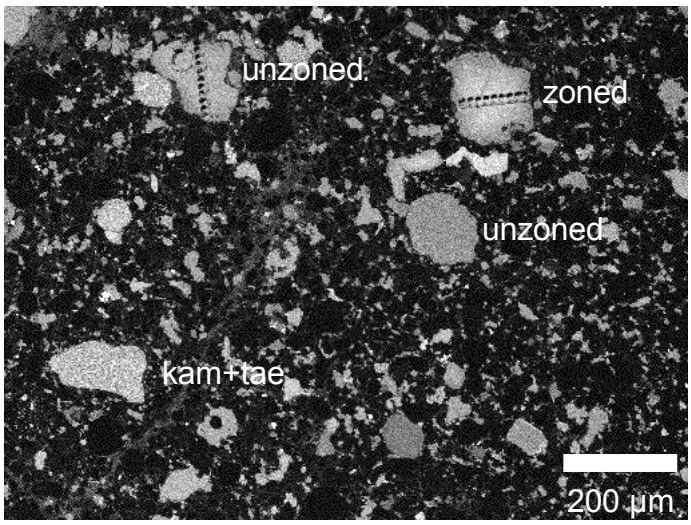

Figure 1

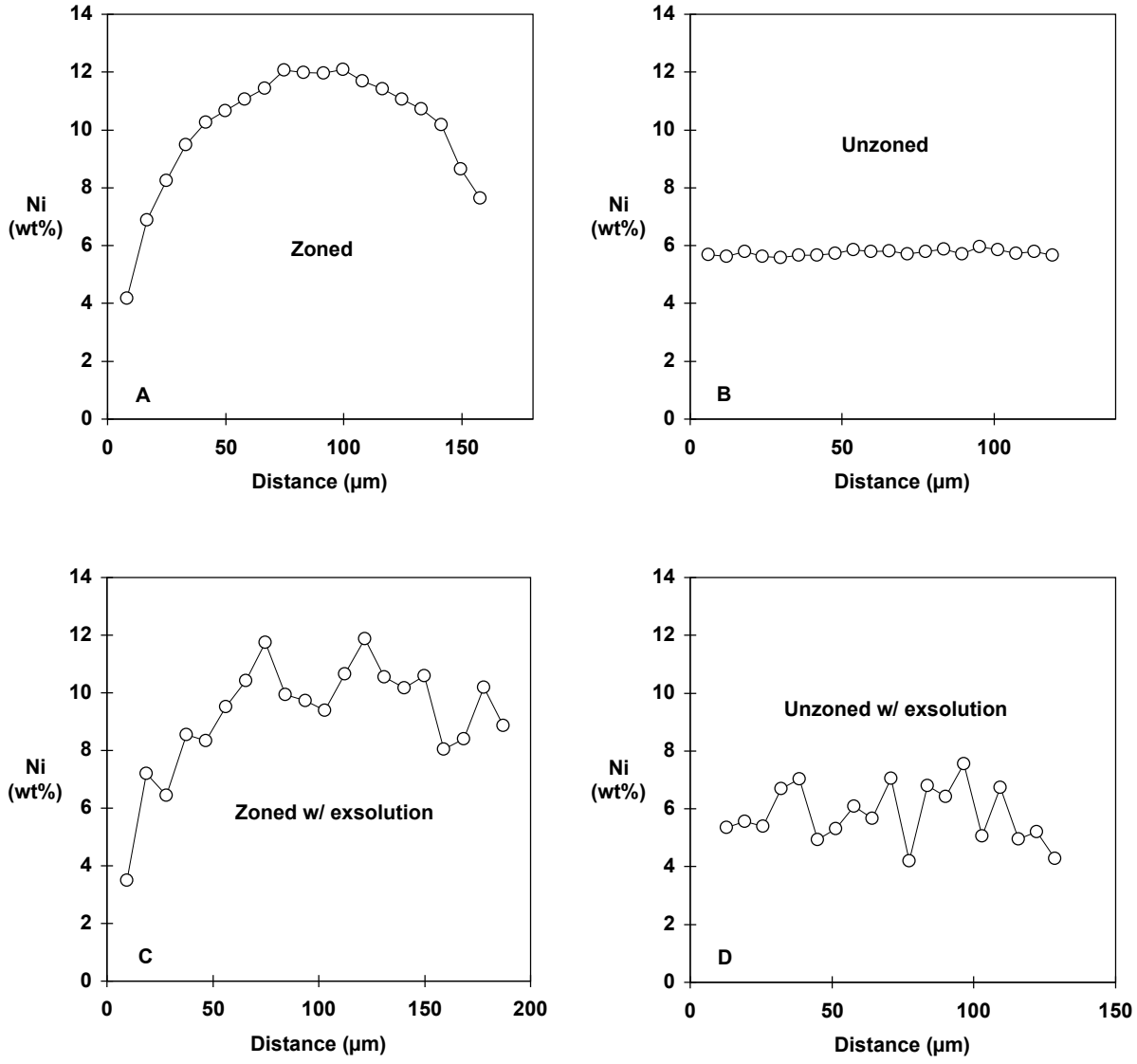
Ni (wt%)
Distance (μm)
Zoned
A
Unzoned
B
Zoned w/ exsolution
C
Unzoned w/ exsolution
D

Figure 2

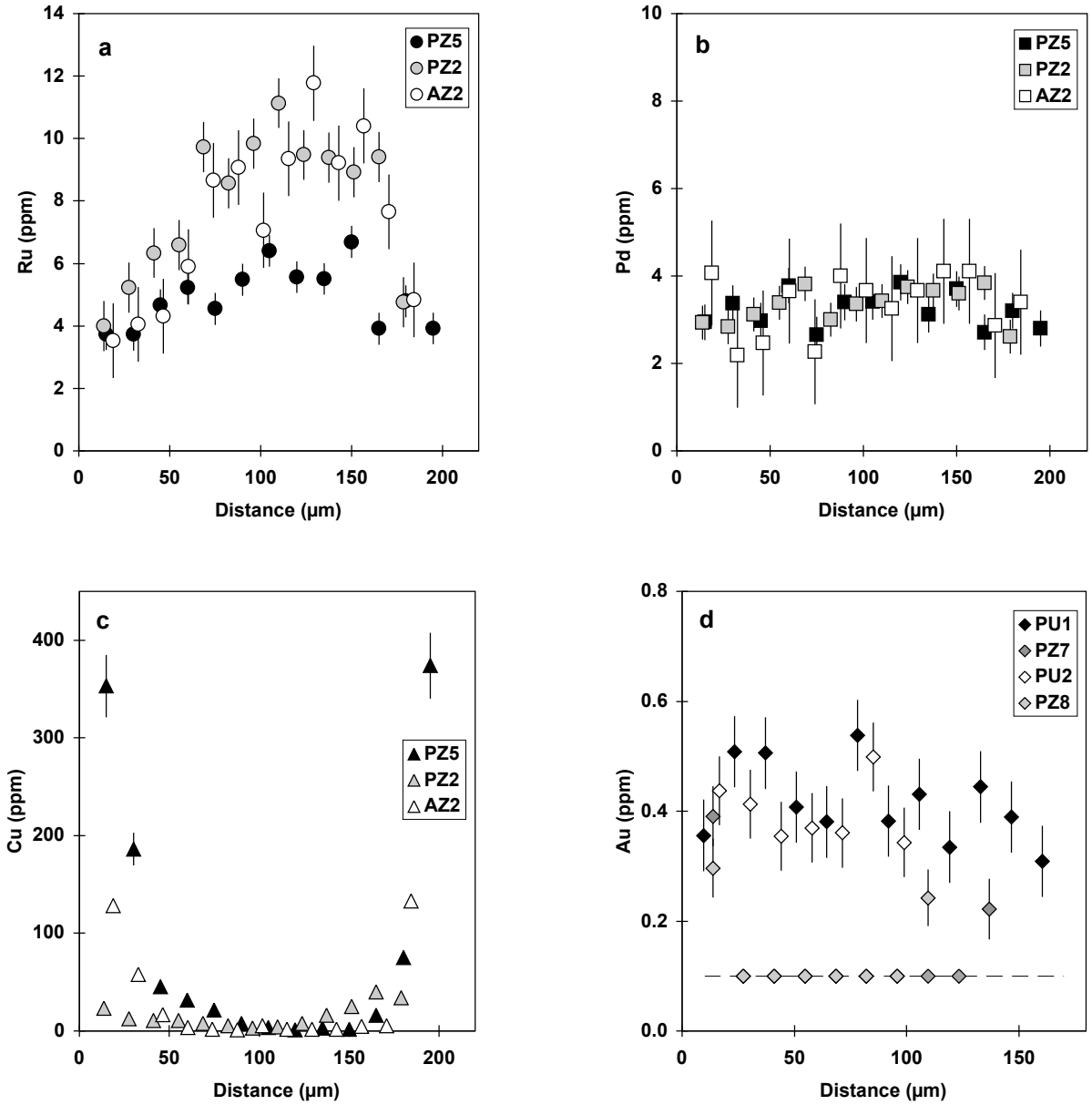
a
PZ5
PZ2
AZ2
Ru (ppm)
Distance (µm)
b
PZ5
PZ2
AZ2
Pd (ppm)
Distance (µm)
c
PZ5
PZ2
AZ2
Cu (ppm)
Distance (µm)
d
PU1
PZ7
PU2
PZ8
Au (ppm)
Distance (µm)

Figure 3

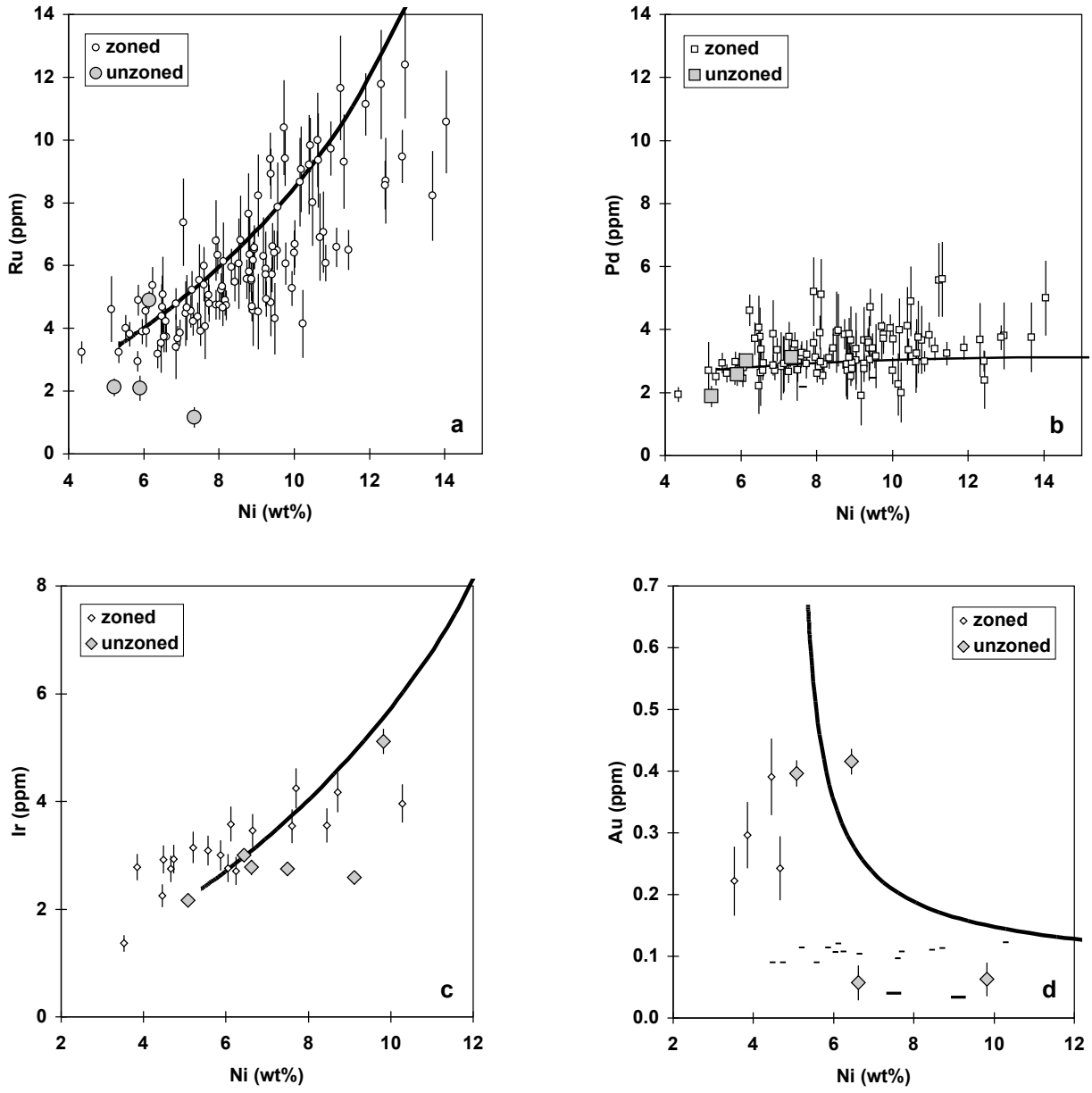

Figure 4

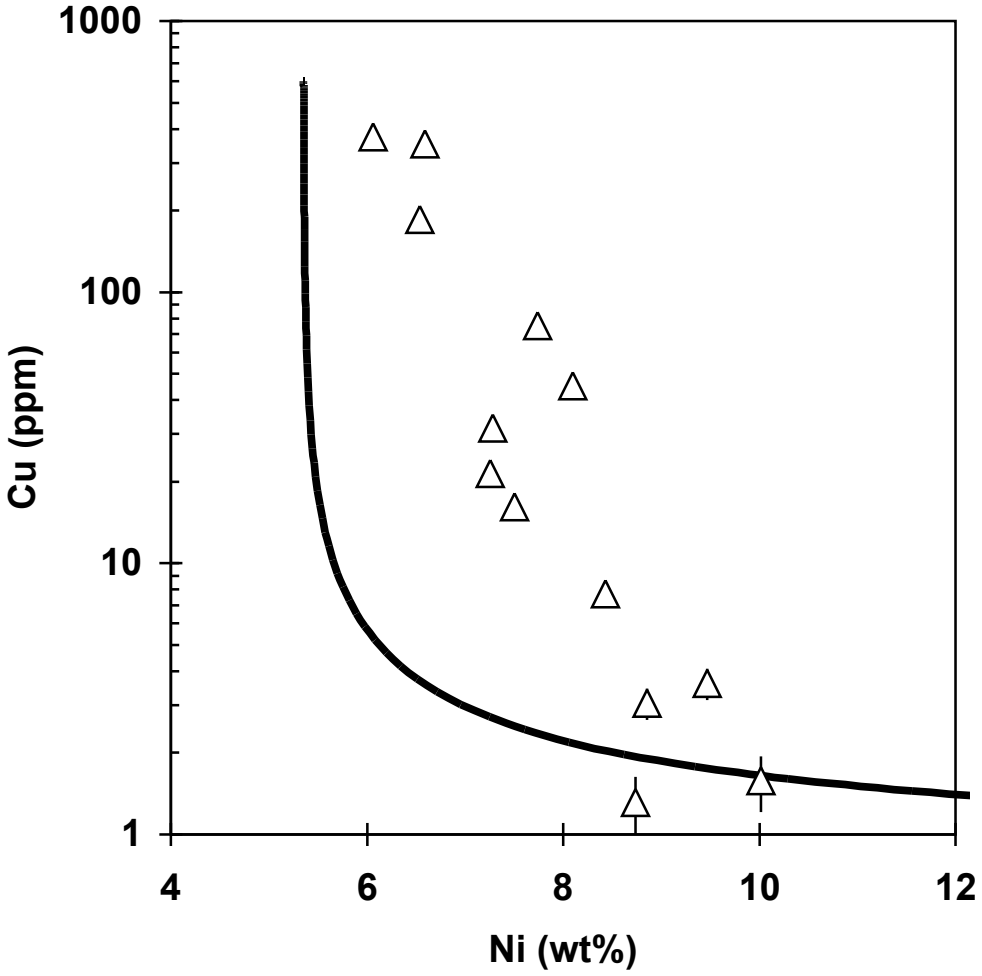

Figure 5

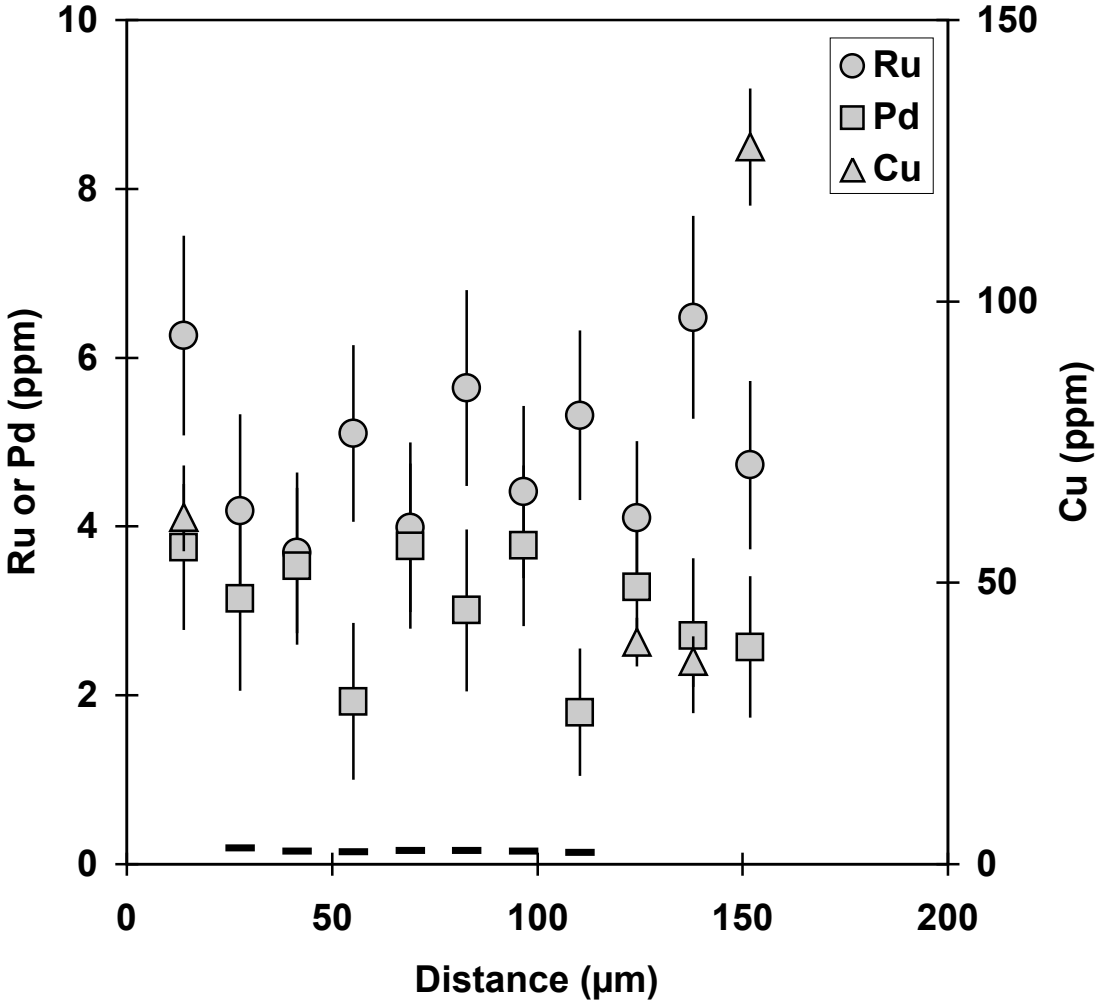
Ru
Pd
Cu
Ru or Pd (ppm)
Cu (ppm)
Distance (μm)
0
2
4
6
8
10
0
50
100
150
0
50
100
150
200

Figure 6

Two Models of Zoned Grain Growth
(Campbell et al., 2001)

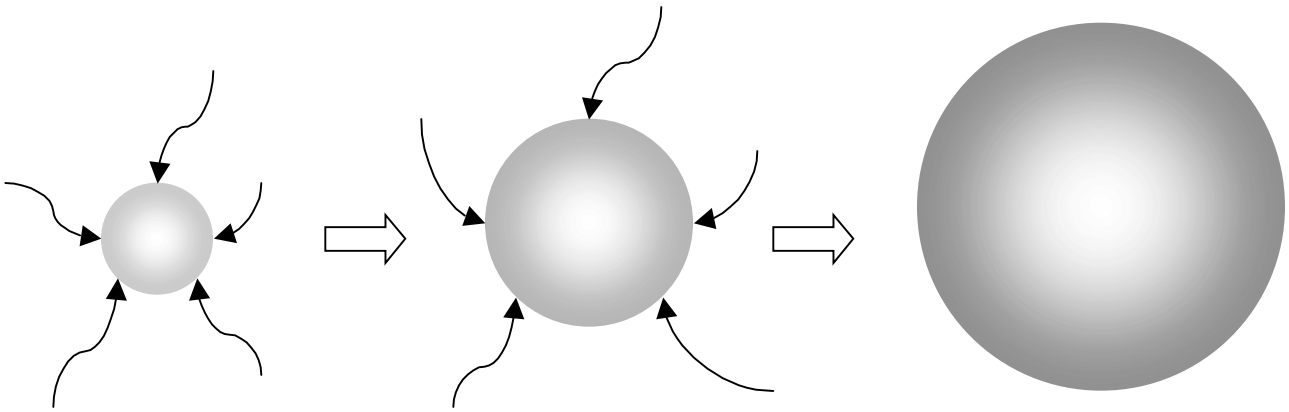

1. Condensation from a cooling gas

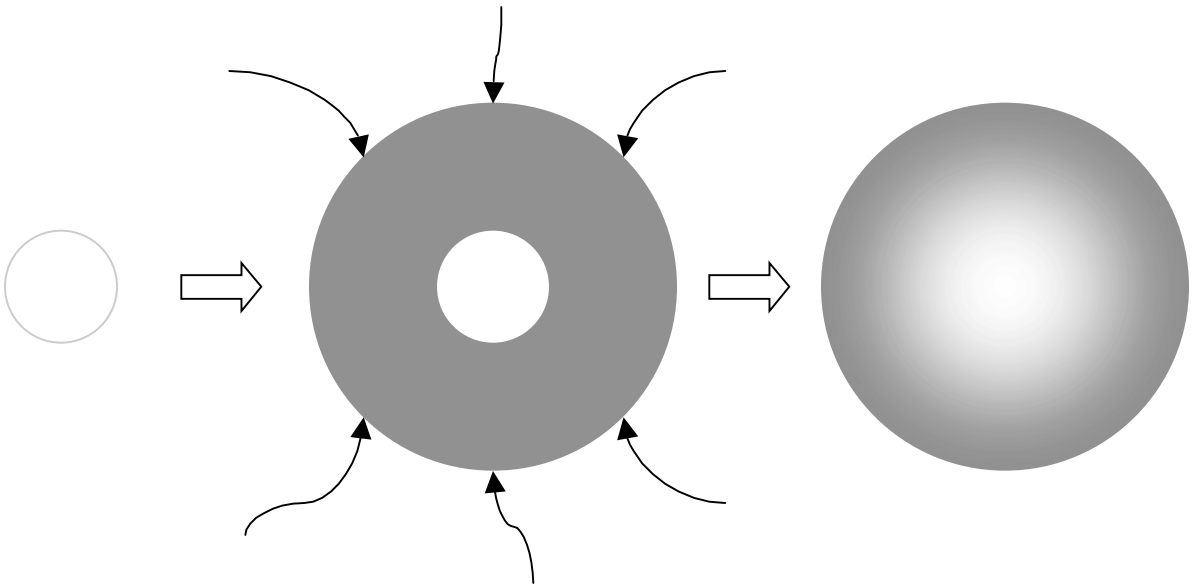

2. Deposition onto a refractory core, plus diffusion

Figure 7

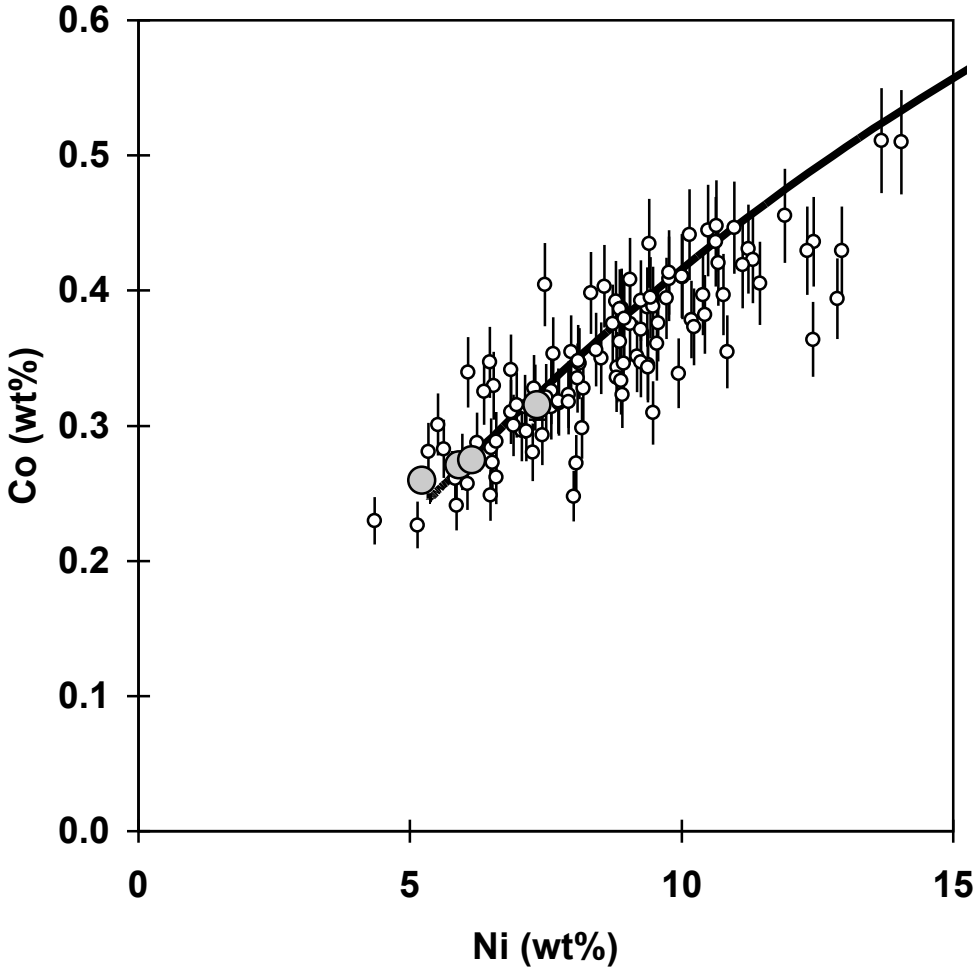

Figure 8

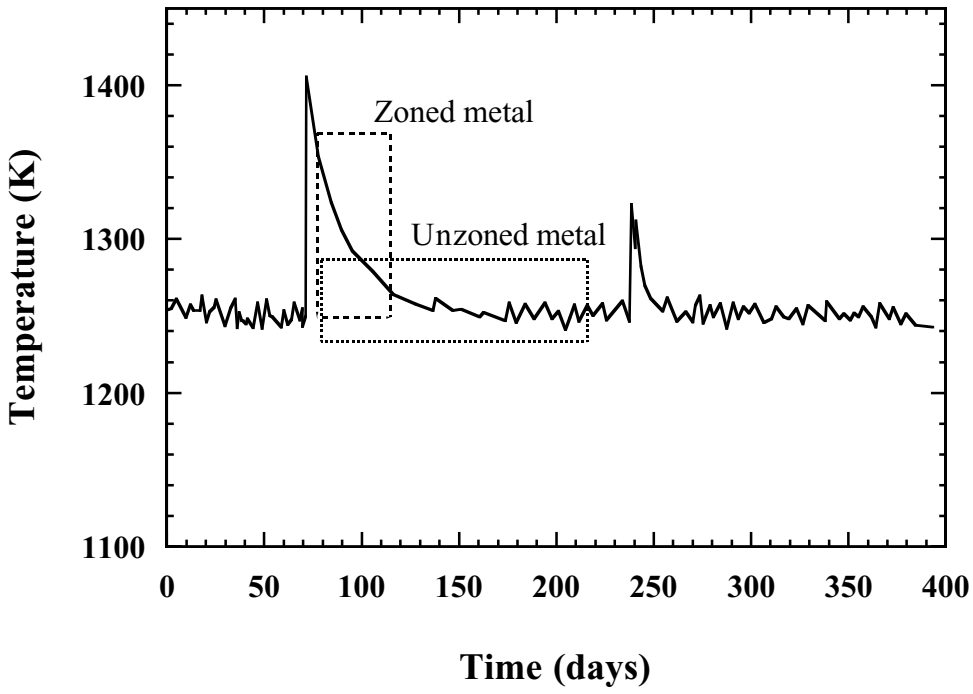
Temperature (K)
1400
1300
1200
1100
Zoned metal
Unzoned metal
0
50
100
150
200
250
300
350
400
Time (days)

Figure 9

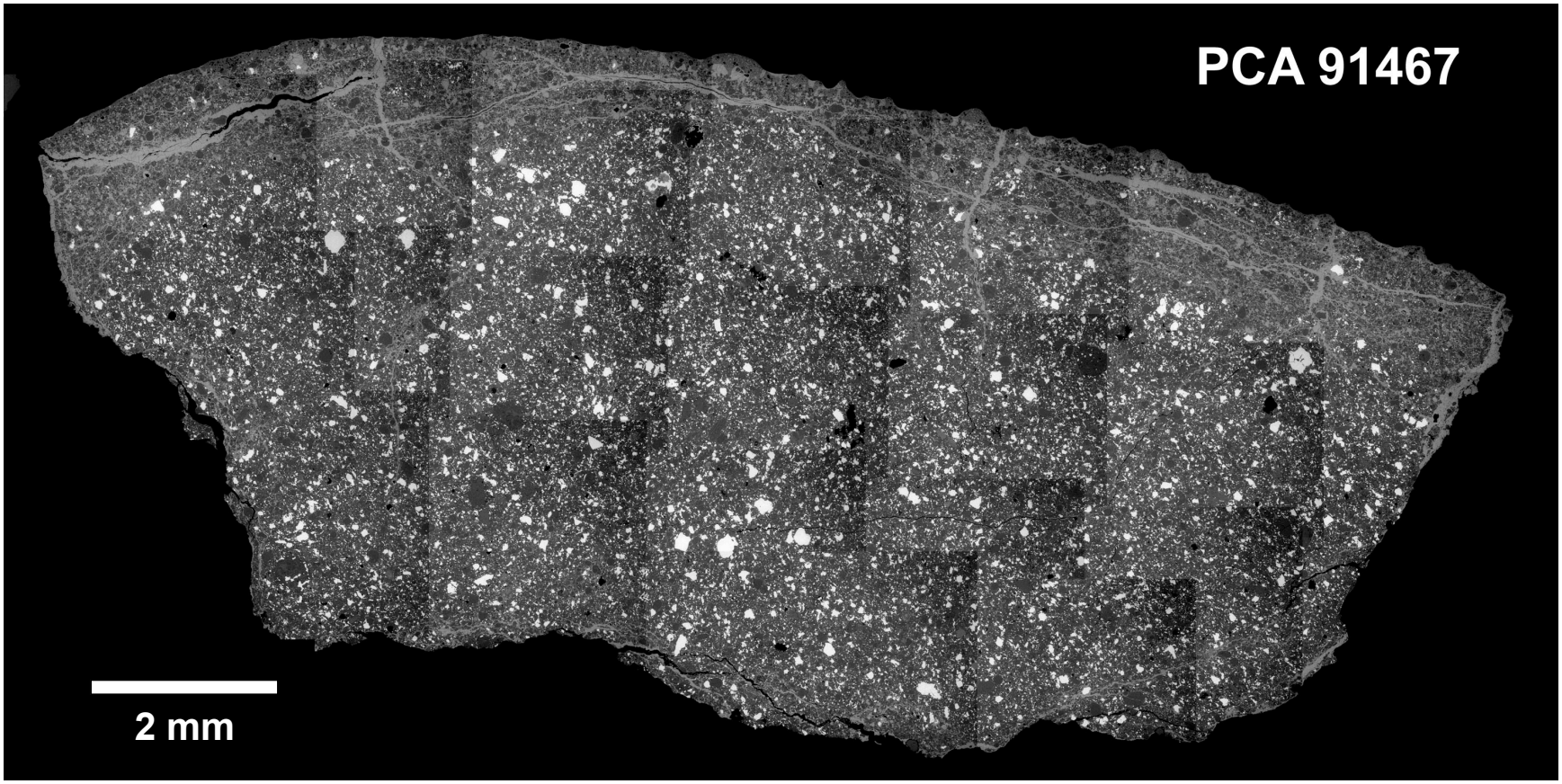

Figure EA1

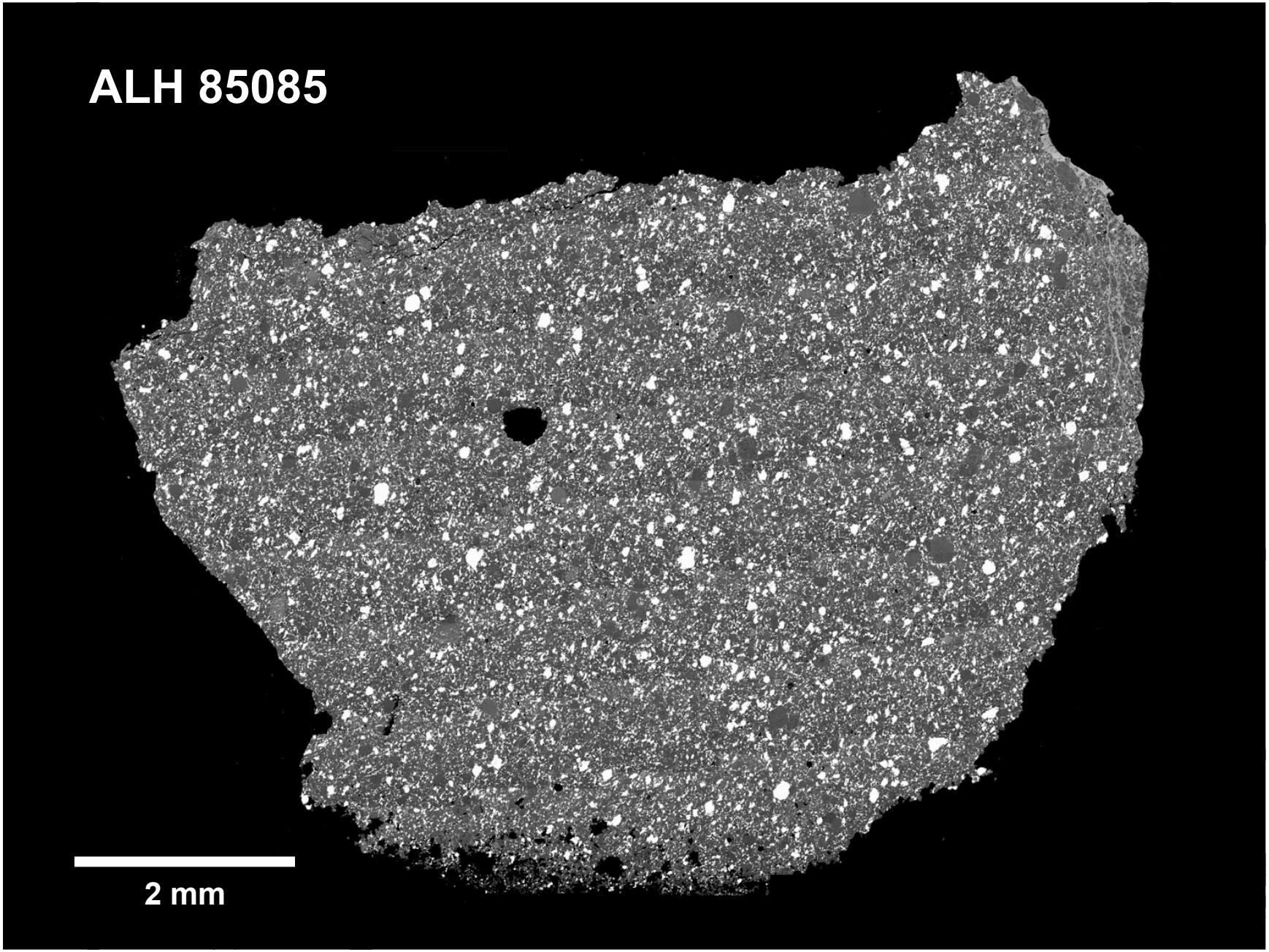

Figure EA2

Table EA3. LA-ICP-MS analyses across zoned metal grains. Underlined entries denote detection limits.
In each grain label, A = ALH 85085; P = PCA 91467; Z = zoned; U = unzoned.

#AZ1:	µm	Fe, wt%	Co, wt%	Ni, wt%	Cu, ppm	Ru, ppm	Pd ppm
	14	93.2 ± 0.5	0.28 ± 0.02	6.5 ± 0.5	95 ± 8	4.7 ± 1.0	3.8 ± 0.9
	28	90.6 ± 0.7	0.38 ± 0.03	9.0 ± 0.7	4	8.2 ± 1.3	3.0 ± 0.9
	42	88.9 ± 0.8	0.44 ± 0.03	10.6 ± 0.8	5	10.0 ± 1.5	3.0 ± 1.0
	56	87.1 ± 0.9	0.44 ± 0.03	12.4 ± 0.9	4	8.7 ± 1.4	2.4 ± 0.9
	71	85.8 ± 1.0	0.51 ± 0.04	13.7 ± 1.0	5	8.2 ± 1.4	3.7 ± 1.1
	85	86.6 ± 1.0	0.43 ± 0.03	12.9 ± 1.0	5	12.4 ± 1.7	3.8 ± 1.1
	99	85.4 ± 1.1	0.51 ± 0.04	14.0 ± 1.1	5	10.6 ± 1.6	5.0 ± 1.2
	113	88.3 ± 0.9	0.43 ± 0.03	11.2 ± 0.9	5	11.7 ± 1.7	5.6 ± 1.2
	127	88.3 ± 0.9	0.42 ± 0.03	11.3 ± 0.9	5	9.3 ± 1.5	5.6 ± 1.2
	141	89.1 ± 0.8	0.44 ± 0.03	10.5 ± 0.8	5	8.0 ± 1.4	4.9 ± 1.1
	155	92.1 ± 0.6	0.40 ± 0.03	7.5 ± 0.6	4	5.5 ± 1.2	2.7 ± 1.0

#AZ2:	µm	Fe, wt%	Co, wt%	Ni, wt%	Cu, ppm	Ru, ppm	Pd ppm
	14	93.2 ± 0.5	0.35 ± 0.03	6.5 ± 0.5	128 ± 11	3.5 ± 0.9	4.1 ± 1.0
	28	92.0 ± 0.6	0.35 ± 0.03	7.6 ± 0.6	58 ± 6	4.1 ± 1.0	2.2
	41	90.2 ± 0.7	0.31 ± 0.02	9.5 ± 0.7	17 ± 4	4.3 ± 1.1	2.5
	55	90.4 ± 0.7	0.37 ± 0.03	9.2 ± 0.7	4 ± 4	5.9 ± 1.2	3.7 ± 1.1
	69	89.4 ± 0.8	0.44 ± 0.03	10.1 ± 0.8	2	8.7 ± 1.4	2.3 ± 1.0
	83	89.4 ± 0.8	0.38 ± 0.03	10.2 ± 0.8	1	9.1 ± 1.4	4.0 ± 1.0
	97	88.8 ± 0.8	0.40 ± 0.03	10.8 ± 0.8	6 ± 4	7.1 ± 1.3	3.7 ± 1.1
	110	88.9 ± 0.8	0.45 ± 0.03	10.6 ± 0.8	2	9.3 ± 1.5	3.2 ± 1.1
	124	87.3 ± 0.9	0.43 ± 0.03	12.3 ± 0.9	2	11.8 ± 1.7	3.7 ± 1.2
	138	89.2 ± 0.8	0.40 ± 0.03	10.4 ± 0.8	2	9.2 ± 1.6	4.1 ± 1.2
	152	89.9 ± 0.7	0.39 ± 0.03	9.7 ± 0.7	5 ± 3	10.4 ± 1.5	4.1 ± 1.0
	166	90.8 ± 0.7	0.39 ± 0.03	8.8 ± 0.7	5 ± 3	7.7 ± 1.3	2.9 ± 1.0
	179	90.3 ± 0.7	0.35 ± 0.03	9.4 ± 0.7	133 ± 11	4.8 ± 1.1	3.4 ± 1.0

#AZ3:	µm	Fe, wt%	Co, wt%	Ni, wt%	Cu, ppm	Ru, ppm	Pd ppm
	14	92.8 ± 0.5	0.31 ± 0.02	6.9 ± 0.5	8	3.4 ± 1.0	3.9 ± 1.1
	28	90.8 ± 0.7	0.34 ± 0.03	8.8 ± 0.7	7	6.4 ± 1.2	2.7 ± 0.9
	41	91.5 ± 0.6	0.35 ± 0.03	8.1 ± 0.6	8	6.1 ± 1.2	5.1 ± 1.1
	55	89.4 ± 0.8	0.37 ± 0.03	10.2 ± 0.8	8	4.1 ± 1.1	2.0 ± 1.0
	69	88.9 ± 0.8	0.42 ± 0.03	10.7 ± 0.8	8	6.9 ± 1.4	3.8 ± 1.2
	83	90.7 ± 0.7	0.39 ± 0.03	8.9 ± 0.7	8	4.6 ± 1.1	3.7 ± 1.1
	97	92.6 ± 0.5	0.31 ± 0.02	7.1 ± 0.5	7	4.5 ± 1.0	2.9 ± 0.9

#AZ4:	µm	Fe, wt%	Co, wt%	Ni, wt%	Cu, ppm	Ru, ppm	Pd ppm
	14	93.2 ± 0.5	0.27 ± 0.02	6.5 ± 0.5	9	5.1 ± 1.2	2.6 ± 1.0
	28	92.6 ± 0.5	0.30 ± 0.02	7.1 ± 0.5	9	7.4 ± 1.4	2.8 ± 1.1
	42	90.5 ± 0.7	0.35 ± 0.03	9.2 ± 0.7	8	6.3 ± 1.2	1.9 ± 0.9
	56	90.5 ± 0.7	0.41 ± 0.03	9.0 ± 0.7	9	4.5 ± 1.2	3.4 ± 1.1
	71	90.9 ± 0.7	0.34 ± 0.03	8.8 ± 0.7	9	5.8 ± 1.3	2.9 ± 1.1
	85	91.1 ± 0.6	0.35 ± 0.03	8.5 ± 0.6	11	6.1 ± 1.4	3.9 ± 1.3
	99	93.3 ± 0.5	0.25 ± 0.02	6.5 ± 0.5	7	4.4 ± 1.0	2.2 ± 0.9
	113	94.6 ± 0.4	0.23 ± 0.02	5.1 ± 0.4	8	4.6 ± 1.0	2.7 ± 0.9

#AZ5:	µm	Fe, wt%	Co, wt%	Ni, wt%	Cu, ppm	Ru, ppm	Pd ppm
	14	92.6 ± 0.5	0.30 ± 0.02	7.1 ± 0.5	3.5	4.7 ± 1.0	2.9 ± 0.9
	28	91.0 ± 0.7	0.40 ± 0.03	8.6 ± 0.7	4.5	6.8 ± 1.4	4.0 ± 1.2
	41	90.1 ± 0.7	0.38 ± 0.03	9.6 ± 0.7	4.1	7.9 ± 1.4	3.2 ± 1.0
	55	91.8 ± 0.6	0.32 ± 0.02	7.9 ± 0.6	3.9	6.8 ± 1.3	5.2 ± 1.1

#PZ1:	µm	Fe, wt%	Co, wt%	Ni, wt%	Cu, ppm	Ru, ppm	Pd ppm
	14	95.4 ± 0.3	0.23 ± 0.02	4.4 ± 0.3	176 ± 13	3.2 ± 0.4	1.9 ± 0.2
	28	91.5 ± 0.6	0.30 ± 0.02	8.2 ± 0.6	2	4.9 ± 0.5	2.5 ± 0.3
	41	90.8 ± 0.7	0.32 ± 0.02	8.9 ± 0.7	2	6.2 ± 0.6	2.5 ± 0.3
	55	88.2 ± 0.9	0.41 ± 0.03	11.4 ± 0.9	2	6.5 ± 0.6	3.2 ± 0.4
	69	90.1 ± 0.7	0.36 ± 0.03	9.5 ± 0.7	2	6.5 ± 0.6	3.1 ± 0.3
	83	90.2 ± 0.7	0.43 ± 0.03	9.4 ± 0.7	2	5.7 ± 0.6	3.0 ± 0.3

	96	91.3 ± 0.6	0.40 ± 0.03	8.3 ± 0.6	7 ± 1	6.0 ± 0.6	3.1 ± 0.3
	110	88.8 ± 0.8	0.35 ± 0.03	10.8 ± 0.8	15 ± 1	6.1 ± 0.6	3.0 ± 0.3
	124	90.4 ± 0.7	0.35 ± 0.03	9.2 ± 0.7	50 ± 4	5.7 ± 0.5	2.9 ± 0.3
	138	90.7 ± 0.7	0.35 ± 0.03	8.9 ± 0.7	8 ± 1	6.5 ± 0.6	3.0 ± 0.3
	151	91.8 ± 0.6	0.32 ± 0.02	7.9 ± 0.6	22 ± 2	4.8 ± 0.5	3.6 ± 0.4
	165	93.5 ± 0.5	0.29 ± 0.02	6.2 ± 0.5	610 ± 46	5.4 ± 0.6	4.6 ± 0.5
#PZ2:	µm	Fe, wt%	Co, wt%	Ni, wt%	Cu, ppm	Ru, ppm	Pd ppm
	14	94.2 ± 0.4	0.30 ± 0.02	5.5 ± 0.4	23.2 ± 1.9	4.0 ± 0.4	2.9 ± 0.3
	28	91.7 ± 0.6	0.27 ± 0.02	8.1 ± 0.6	12.7 ± 1.1	5.2 ± 0.5	2.8 ± 0.3
	41	91.7 ± 0.6	0.35 ± 0.03	8.0 ± 0.6	10.7 ± 1.0	6.3 ± 0.6	3.1 ± 0.3
	55	88.5 ± 0.8	0.42 ± 0.03	11.1 ± 0.8	11.0 ± 1.0	6.6 ± 0.6	3.4 ± 0.4
	69	88.6 ± 0.8	0.45 ± 0.03	11.0 ± 0.8	7.6 ± 0.8	9.7 ± 0.9	3.8 ± 0.4
	83	87.2 ± 0.9	0.36 ± 0.03	12.4 ± 0.9	5.3 ± 0.7	8.6 ± 0.8	3.0 ± 0.3
	96	89.2 ± 0.8	0.38 ± 0.03	10.4 ± 0.8	2.9 ± 0.5	9.8 ± 0.9	3.4 ± 0.4
	110	87.6 ± 0.9	0.46 ± 0.03	11.9 ± 0.9	4.1 ± 0.6	11.1 ± 1.0	3.4 ± 0.4
	124	86.7 ± 1.0	0.39 ± 0.03	12.9 ± 1.0	8.0 ± 0.8	9.5 ± 0.8	3.7 ± 0.4
	138	90.3 ± 0.7	0.39 ± 0.03	9.4 ± 0.7	15.9 ± 1.4	9.4 ± 0.8	3.7 ± 0.4
	151	90.3 ± 0.7	0.34 ± 0.03	9.4 ± 0.7	25.3 ± 2.0	8.9 ± 0.8	3.6 ± 0.4
	165	89.8 ± 0.7	0.41 ± 0.03	9.8 ± 0.7	39.7 ± 3.2	9.4 ± 0.9	3.8 ± 0.4
	179	91.7 ± 0.6	0.25 ± 0.02	8.0 ± 0.6	33.8 ± 2.7	4.8 ± 0.5	2.6 ± 0.3
#PZ3:	µm	Fe, wt%	Co, wt%	Ni, wt%	Cu, ppm	Ru, ppm	Pd ppm
	14	94.4 ± 0.4	0.28 ± 0.02	5.3 ± 0.4	60.1 ± 4.6	3.2 ± 0.3	2.5 ± 0.3
	28	92.8 ± 0.5	0.30 ± 0.02	6.9 ± 0.5	138.8 ± 10.6	3.7 ± 0.4	2.7 ± 0.3
	41	92.7 ± 0.5	0.32 ± 0.02	7.0 ± 0.5	32.3 ± 2.6	3.9 ± 0.4	3.4 ± 0.4
	55	92.3 ± 0.6	0.29 ± 0.02	7.4 ± 0.6	26.9 ± 2.2	4.4 ± 0.5	3.5 ± 0.4
	69	92.4 ± 0.6	0.32 ± 0.02	7.3 ± 0.6	27.3 ± 2.2	4.2 ± 0.4	3.2 ± 0.4
	83	94.1 ± 0.4	0.28 ± 0.02	5.6 ± 0.4	22.0 ± 1.8	3.8 ± 0.4	2.6 ± 0.3
	96	93.1 ± 0.5	0.29 ± 0.02	6.6 ± 0.5	24.4 ± 2.0	4.2 ± 0.4	2.7 ± 0.3
	110	93.8 ± 0.5	0.27 ± 0.02	6.0 ± 0.5	26.2 ± 2.1	3.9 ± 0.4	2.9 ± 0.3
	124	93.9 ± 0.4	0.26 ± 0.02	5.8 ± 0.4	26.0 ± 2.1	2.9 ± 0.3	2.5 ± 0.3
#PZ4:	µm	Fe, wt%	Co, wt%	Ni, wt%	Cu, ppm	Ru, ppm	Pd ppm
	14	93.9 ± 0.4	0.24 ± 0.02	5.9 ± 0.4	28.4 ± 2.3	4.9 ± 0.5	3.0 ± 0.3
	28	93.7 ± 0.5	0.26 ± 0.02	6.1 ± 0.5	1.7 ± 0.4	4.6 ± 0.5	2.5 ± 0.3
	41	92.1 ± 0.6	0.33 ± 0.02	7.6 ± 0.6	1.4 ± 0.6	6.0 ± 0.6	3.1 ± 0.4
	55	89.7 ± 0.8	0.34 ± 0.03	9.9 ± 0.8	1.4 ± 0.6	5.3 ± 0.6	4.0 ± 0.4
	69	90.8 ± 0.7	0.33 ± 0.03	8.9 ± 0.7	1.5 ± 0.5	4.7 ± 0.5	3.1 ± 0.3
	83	91.5 ± 0.6	0.33 ± 0.02	8.2 ± 0.6	1.1	4.7 ± 0.5	2.9 ± 0.3
	96	92.1 ± 0.6	0.31 ± 0.02	7.6 ± 0.6	1.6 ± 0.5	5.4 ± 0.5	3.3 ± 0.4
	110	92.8 ± 0.5	0.34 ± 0.03	6.9 ± 0.5	1.3 ± 0.5	4.8 ± 0.5	2.9 ± 0.3
#PZ5:	µm	Fe, wt%	Co, wt%	Ni, wt%	Cu, ppm	Ru, ppm	Pd ppm
	15	93.1 ± 0.5	0.26 ± 0.02	6.6 ± 0.5	353.2 ± 26.9	3.7 ± 0.5	2.9 ± 0.4
	30	93.1 ± 0.5	0.33 ± 0.03	6.5 ± 0.5	186.0 ± 14.2	3.7 ± 0.5	3.4 ± 0.5
	45	91.5 ± 0.6	0.35 ± 0.03	8.1 ± 0.6	45.2 ± 3.5	4.7 ± 0.6	3.0 ± 0.4
	60	92.4 ± 0.6	0.33 ± 0.02	7.3 ± 0.6	31.5 ± 2.5	5.2 ± 0.6	3.8 ± 0.5
	75	92.5 ± 0.6	0.28 ± 0.02	7.3 ± 0.6	21.5 ± 1.7	4.6 ± 0.5	2.7 ± 0.4
	90	91.2 ± 0.6	0.36 ± 0.03	8.4 ± 0.6	7.7 ± 0.7	5.5 ± 0.6	3.4 ± 0.5
	105	90.1 ± 0.7	0.39 ± 0.03	9.5 ± 0.7	3.6 ± 0.5	6.4 ± 0.7	3.4 ± 0.5
	120	90.9 ± 0.7	0.38 ± 0.03	8.7 ± 0.7	1.3 ± 0.3	5.6 ± 0.6	3.9 ± 0.5
	135	90.8 ± 0.7	0.36 ± 0.03	8.9 ± 0.7	3.0 ± 0.4	5.5 ± 0.6	3.1 ± 0.4
	150	89.6 ± 0.8	0.41 ± 0.03	10.0 ± 0.8	1.6 ± 0.4	6.7 ± 0.8	3.7 ± 0.5
	165	92.2 ± 0.6	0.32 ± 0.02	7.5 ± 0.6	16.2 ± 1.3	3.9 ± 0.5	2.7 ± 0.4
	180	91.9 ± 0.6	0.32 ± 0.02	7.7 ± 0.6	75.2 ± 5.8	4.8 ± 0.6	3.2 ± 0.5
	195	93.6 ± 0.5	0.34 ± 0.03	6.1 ± 0.5	373.9 ± 28.5	3.9 ± 0.5	2.8 ± 0.4
#PZ6:	µm	Fe, wt%	Co, wt%	Ni, wt%	Cu, ppm	Ru, ppm	Pd ppm
	15	93.3 ± 0.5	0.33 ± 0.02	6.4 ± 0.5	143.9 ± 11.0	3.2 ± 0.4	3.7 ± 0.5
	30	91.6 ± 0.6	0.34 ± 0.03	8.1 ± 0.6	21.5 ± 1.8	5.3 ± 0.6	3.9 ± 0.5
	45	90.8 ± 0.7	0.39 ± 0.03	8.9 ± 0.7	9.8 ± 0.9	5.6 ± 0.6	3.9 ± 0.5
	60	90.4 ± 0.7	0.39 ± 0.03	9.3 ± 0.7	4.9 ± 0.5	4.9 ± 0.6	2.8 ± 0.4

Table EA3

75	89.8 ± 0.7	0.41 ± 0.03	9.8 ± 0.7	10.6 ± 0.9	6.1 ± 0.7	3.7 ± 0.5
90	90.2 ± 0.7	0.39 ± 0.03	9.4 ± 0.7	26.5 ± 2.1	6.6 ± 0.7	4.7 ± 0.6
105	89.6 ± 0.8	0.41 ± 0.03	10.0 ± 0.8	14.6 ± 1.2	6.4 ± 0.7	2.7 ± 0.4
120	90.7 ± 0.7	0.38 ± 0.03	8.9 ± 0.7	4.7 ± 0.5	6.6 ± 0.7	2.8 ± 0.4
135	92.0 ± 0.6	0.32 ± 0.02	7.7 ± 0.6	50.7 ± 4.0	5.1 ± 0.6	2.9 ± 0.5

#PZ7:	µm	Cr, wt%	Fe, wt%	Ni, wt%	Ir, ppm	Au, ppm
	14	0.148 ± 0.011	95.40 ± 0.3	4.5 ± 0.3	2.3 ± 0.2	0.39 ± 0.06
	27	0.142 ± 0.011	91.40 ± 0.6	8.5 ± 0.6	3.6 ± 0.3	<u>0.11</u>
	41	0.132 ± 0.010	92.17 ± 0.6	7.7 ± 0.6	4.2 ± 0.4	<u>0.11</u>
	55	0.138 ± 0.011	89.58 ± 0.8	10.3 ± 0.8	4.0 ± 0.4	<u>0.12</u>
	69	0.105 ± 0.008	92.30 ± 0.6	7.6 ± 0.6	3.5 ± 0.3	<u>0.10</u>
	82	0.131 ± 0.010	91.16 ± 0.7	8.7 ± 0.7	4.2 ± 0.4	<u>0.11</u>
	96	0.126 ± 0.010	93.23 ± 0.5	6.6 ± 0.5	3.5 ± 0.3	<u>0.10</u>
	110	0.121 ± 0.009	93.83 ± 0.5	6.0 ± 0.5	2.8 ± 0.3	<u>0.11</u>
	123	0.194 ± 0.015	93.56 ± 0.5	6.2 ± 0.5	2.7 ± 0.3	<u>0.11</u>
	137	0.188 ± 0.014	96.28 ± 0.3	3.5 ± 0.3	1.4 ± 0.2	0.22 ± 0.06

#PZ8:	µm	Cr, wt%	Fe, wt%	Ni, wt%	Ir, ppm	Au, ppm
	14	0.291 ± 0.022	95.86 ± 0.3	3.8 ± 0.3	2.8 ± 0.2	0.30 ± 0.05
	27	0.229 ± 0.017	95.29 ± 0.3	4.5 ± 0.3	2.9 ± 0.3	<u>0.10</u>
	41	0.269 ± 0.020	94.16 ± 0.4	5.6 ± 0.4	3.1 ± 0.3	<u>0.10</u>
	55	0.226 ± 0.017	95.04 ± 0.4	4.7 ± 0.4	2.9 ± 0.3	<u>0.10</u>
	69	0.259 ± 0.020	94.53 ± 0.4	5.2 ± 0.4	3.1 ± 0.3	<u>0.10</u>
	82	0.211 ± 0.016	93.92 ± 0.4	5.9 ± 0.4	3.0 ± 0.3	<u>0.10</u>
	96	0.259 ± 0.020	93.63 ± 0.5	6.1 ± 0.5	3.6 ± 0.3	<u>0.10</u>
	110	0.208 ± 0.016	95.13 ± 0.4	4.7 ± 0.4	2.7 ± 0.2	0.24 ± 0.05

Table EA3

Table EA4. LA-ICP-MS analyses across unzoned metal grains. Underlined entries denote detection limits.

#AU1	µm	Fe, wt%	Co, wt%	Ni, wt%	Cu, ppm	Ru, ppm	Pd, ppm
	14	92.3 ± 0.6	0.29 ± 0.02	7.4 ± 0.6	51 ± 5	2.1	2.6 ± 0.8
	28	92.4 ± 0.6	0.29 ± 0.02	7.3 ± 0.6	17 ± 4	3.0	4.0 ± 1.1
	41	92.2 ± 0.6	0.35 ± 0.03	7.5 ± 0.6	16 ± 5	3.6	4.6 ± 1.4
	55	91.6 ± 0.6	0.38 ± 0.03	8.1 ± 0.6	12 ± 4	3.2	3.5 ± 1.2
	69	92.7 ± 0.5	0.34 ± 0.03	6.9 ± 0.5	9 ± 4	2.8	2.8 ± 1.0
	83	91.2 ± 0.6	0.34 ± 0.03	8.4 ± 0.6	15 ± 4	2.9	2.3 ± 1.0
	97	92.6 ± 0.5	0.31 ± 0.02	7.1 ± 0.5	6 ± 4	2.7	2.6 ± 1.0
	110	93.1 ± 0.5	0.30 ± 0.02	6.6 ± 0.5	13 ± 4	2.9	3.2 ± 1.1
	124	92.4 ± 0.6	0.28 ± 0.02	7.3 ± 0.6	17 ± 4	2.6	2.7 ± 1.0
	138	93.0 ± 0.5	0.27 ± 0.02	6.7 ± 0.5	18 ± 4	2.4	3.0 ± 0.9
	AVG	92.3 ± 0.2	0.316 ± 0.011	7.3 ± 0.2	17 ± 4	1.2 ± 0.3	3.1 ± 0.2

#AU2	µm	Fe, wt%	Co, wt%	Ni, wt%	Cu, ppm	Ru, ppm	Pd, ppm
	14	92.6 ± 0.5	0.32 ± 0.02	7.0 ± 0.5	69 ± 7	1.1	2.0
	28	93.4 ± 0.5	0.24 ± 0.02	6.4 ± 0.5	23 ± 4	2.9 ± 1.0	4.1 ± 1.1
	41	94.9 ± 0.4	0.26 ± 0.02	4.9 ± 0.4	12 ± 4	1.1 ± 0.8	1.9 ± 0.9
	55	94.6 ± 0.4	0.28 ± 0.02	5.1 ± 0.4	1	1.1	3.9 ± 1.1
	69	93.1 ± 0.5	0.28 ± 0.02	6.6 ± 0.5	11 ± 4	2.7 ± 0.9	2.4 ± 0.9
	83	93.6 ± 0.5	0.26 ± 0.02	6.2 ± 0.5	17 ± 4	3.7 ± 1.0	1.8
	97	95.0 ± 0.4	0.24 ± 0.02	4.8 ± 0.4	27 ± 4	1.0	2.7 ± 0.9
	110	93.5 ± 0.5	0.28 ± 0.02	6.2 ± 0.5	109 ± 10	3.2 ± 1.2	2.5 ± 1.1
	AVG	93.8 ± 0.3	0.271 ± 0.010	5.9 ± 0.3	35 ± 13	2.1 ± 0.4	2.6 ± 0.4

#AU3	µm	Fe, wt%	Co, wt%	Ni, wt%	Cu, ppm	Ru, ppm	Pd, ppm
	14	94.8 ± 0.4	0.246 ± 0.019	4.9 ± 0.4	243 ± 19	1.8 ± 0.6	1.0
	28	94.8 ± 0.4	0.275 ± 0.021	4.9 ± 0.4	242 ± 19	2.7 ± 0.8	1.2
	41	95.3 ± 0.3	0.248 ± 0.019	4.5 ± 0.3	247 ± 19	1.7 ± 0.7	1.1
	55	94.6 ± 0.4	0.232 ± 0.018	5.2 ± 0.4	229 ± 18	3.8 ± 0.9	3.0 ± 0.8
	69	94.0 ± 0.4	0.272 ± 0.021	5.8 ± 0.4	268 ± 21	2.7 ± 0.8	1.3 ± 0.8
	83	95.3 ± 0.3	0.249 ± 0.019	4.4 ± 0.3	246 ± 19	2.3 ± 0.7	2.7 ± 0.8
	97	93.7 ± 0.5	0.285 ± 0.022	6.0 ± 0.5	347 ± 27	2.0	3.0 ± 0.9
	110	93.8 ± 0.4	0.276 ± 0.021	5.9 ± 0.4	322 ± 25	1.9	2.4 ± 0.9
	124	94.4 ± 0.4	0.254 ± 0.019	5.3 ± 0.4	439 ± 34	1.8	2.1 ± 0.9
	AVG	94.5 ± 0.2	0.260 ± 0.006	5.2 ± 0.2	287 ± 23	2.1 ± 0.3	1.9 ± 0.3

#AU4	µm	Fe, wt%	Co, wt%	Ni, wt%	Cu, ppm	Ru, ppm	Pd, ppm
	14	93.9 ± 0.4	0.239 ± 0.018	5.9 ± 0.4	62 ± 6	6.3 ± 1.2	3.8 ± 1.0
	28	93.1 ± 0.5	0.311 ± 0.024	6.5 ± 0.5	3	4.2 ± 1.1	3.1 ± 1.1
	41	93.9 ± 0.4	0.279 ± 0.021	5.9 ± 0.4	2	3.7 ± 0.9	3.5 ± 0.9
	55	93.9 ± 0.4	0.291 ± 0.022	5.8 ± 0.4	2	5.1 ± 1.0	1.9 ± 0.9
	69	94.0 ± 0.4	0.279 ± 0.021	5.8 ± 0.4	2	4.0 ± 1.0	3.8 ± 1.0
	83	93.0 ± 0.5	0.305 ± 0.023	6.7 ± 0.5	2	5.6 ± 1.2	3.0 ± 1.0
	97	93.1 ± 0.5	0.275 ± 0.021	6.6 ± 0.5	2	4.4 ± 1.0	3.8 ± 1.0
	110	94.8 ± 0.4	0.273 ± 0.021	4.9 ± 0.4	2	5.3 ± 1.0	1.8 ± 0.8
	124	93.5 ± 0.5	0.232 ± 0.018	6.3 ± 0.5	39 ± 4	4.1 ± 0.9	3.3 ± 0.8
	138	92.6 ± 0.5	0.272 ± 0.009	7.1 ± 0.5	36 ± 4	6.5 ± 1.2	2.7 ± 0.9
	152	93.6 ± 0.5	0.263 ± 0.008	6.1 ± 0.5	127 ± 10	4.7 ± 1.0	2.6 ± 0.8
	AVG	93.6 ± 0.2	0.275 ± 0.007	6.1 ± 0.2	29 ± 11	4.9 ± 0.3	3.0 ± 0.2

#PU1	µm	Cr, wt%	Fe, wt%	Ni, wt%	Ir, ppm	Au, ppm
	14	0.109 ± 0.007	93.4 ± 0.4	6.5 ± 0.4	2.7 ± 0.2	0.36 ± 0.06
	27	0.106 ± 0.007	93.2 ± 0.4	6.7 ± 0.4	3.0 ± 0.3	0.51 ± 0.07
	41	0.098 ± 0.006	93.4 ± 0.4	6.5 ± 0.4	3.1 ± 0.3	0.51 ± 0.07
	55	0.104 ± 0.007	93.2 ± 0.4	6.7 ± 0.4	3.1 ± 0.3	0.41 ± 0.06
	69	0.095 ± 0.006	93.8 ± 0.4	6.1 ± 0.4	2.9 ± 0.2	0.38 ± 0.06
	82	0.111 ± 0.007	93.7 ± 0.4	6.2 ± 0.4	2.5 ± 0.2	0.54 ± 0.08
	96	0.097 ± 0.006	93.2 ± 0.4	6.7 ± 0.4	2.8 ± 0.2	0.38 ± 0.06
	110	0.093 ± 0.006	94.0 ± 0.4	5.9 ± 0.4	3.4 ± 0.3	0.43 ± 0.06
	123	0.098 ± 0.006	94.5 ± 0.4	5.4 ± 0.4	2.8 ± 0.2	0.33 ± 0.05
	137	0.117 ± 0.008	92.5 ± 0.5	7.3 ± 0.5	3.6 ± 0.3	0.44 ± 0.07
	151	0.111 ± 0.007	93.3 ± 0.4	6.6 ± 0.4	2.9 ± 0.2	0.39 ± 0.06
	164	0.101 ± 0.007	93.3 ± 0.4	6.6 ± 0.4	3.0 ± 0.2	0.31 ± 0.05
	AVG	0.103 ± 0.002	93.46 ± 0.14	6.44 ± 0.14	3.00 ± 0.09	0.42 ± 0.02

#PU2	µm	Cr, wt%	Fe, wt%	Ni, wt%	Ir, ppm	Au, ppm
	14	0.405 ± 0.026	94.8 ± 0.3	4.8 ± 0.3	2.2 ± 0.2	0.44 ± 0.07
	27	0.531 ± 0.034	94.1 ± 0.3	5.4 ± 0.3	2.2 ± 0.2	0.41 ± 0.06
	41	0.498 ± 0.032	95.1 ± 0.3	4.4 ± 0.3	2.0 ± 0.2	0.35 ± 0.06
	55	0.573 ± 0.037	94.4 ± 0.3	5.0 ± 0.3	2.6 ± 0.2	0.37 ± 0.06
	69	0.435 ± 0.028	94.8 ± 0.3	4.8 ± 0.3	1.8 ± 0.2	0.36 ± 0.06
	82	0.518 ± 0.034	94.2 ± 0.3	5.3 ± 0.3	2.4 ± 0.2	0.50 ± 0.07
	96	0.327 ± 0.021	93.8 ± 0.4	5.9 ± 0.4	2.1 ± 0.2	0.34 ± 0.06
	AVG	0.470 ± 0.032	94.5 ± 0.2	5.1 ± 0.2	2.16 ± 0.10	0.40 ± 0.02

#PU3	µm	Cr, wt%	Fe, wt%	Ni, wt%	Ir, ppm	Au, ppm
	14	0.158 ± 0.010	91.5 ± 0.5	8.4 ± 0.5	3.2 ± 0.2	0.08
	28	0.159 ± 0.010	91.3 ± 0.5	8.5 ± 0.5	2.4 ± 0.2	0.10
	42	0.127 ± 0.008	89.7 ± 0.7	10.2 ± 0.7	2.4 ± 0.2	0.10
	56	0.119 ± 0.008	91.8 ± 0.5	8.1 ± 0.5	2.2 ± 0.2	0.09
	71	0.130 ± 0.008	89.1 ± 0.7	10.8 ± 0.7	2.7 ± 0.2	0.12
	85	0.127 ± 0.008	91.9 ± 0.5	8.0 ± 0.5	2.3 ± 0.2	0.12
	99	0.146 ± 0.010	90.4 ± 0.6	9.4 ± 0.6	2.7 ± 0.2	0.11
	113	0.116 ± 0.008	91.7 ± 0.5	8.2 ± 0.5	2.5 ± 0.2	0.09
	127	0.156 ± 0.010	89.4 ± 0.7	10.4 ± 0.7	2.9 ± 0.2	0.10
	AVG	0.137 ± 0.006	90.7 ± 0.4	9.1 ± 0.4	2.59 ± 0.11	0.03

#PU4	µm	Cr, wt%	Fe, wt%	Ni, wt%	Ir, ppm	Au, ppm
	14	0.097 ± 0.006	88.2 ± 0.8	11.7 ± 0.8	5.6 ± 0.4	0.14
	28	0.097 ± 0.006	90.7 ± 0.6	9.2 ± 0.6	4.4 ± 0.3	0.13
	42	0.087 ± 0.006	90.3 ± 0.6	9.6 ± 0.6	4.2 ± 0.3	0.18 ± 0.06
	56	0.107 ± 0.007	89.4 ± 0.7	10.5 ± 0.7	6.1 ± 0.5	0.17 ± 0.08
	71	0.087 ± 0.006	91.1 ± 0.6	8.9 ± 0.6	4.7 ± 0.4	0.11
	85	0.098 ± 0.006	90.4 ± 0.6	9.5 ± 0.6	5.4 ± 0.4	0.12
	99	0.075 ± 0.005	90.3 ± 0.6	9.6 ± 0.6	4.9 ± 0.4	0.12
	113	0.096 ± 0.006	91.3 ± 0.6	8.6 ± 0.6	4.6 ± 0.4	0.12
	127	0.085 ± 0.006	89.2 ± 0.7	10.7 ± 0.7	6.4 ± 0.5	0.12
	141	0.073 ± 0.005	90.0 ± 0.6	10.0 ± 0.6	4.9 ± 0.4	0.11
	AVG	0.090 ± 0.003	90.1 ± 0.3	9.8 ± 0.3	5.1 ± 0.2	0.06 ± 0.03

#PU5	µm	Cr, wt%	Fe, wt%	Ni, wt%	Ir, ppm	Au, ppm
	14	0.176 ± 0.011	93.2 ± 0.4	6.6 ± 0.4	2.9 ± 0.2	0.22 ± 0.06
	27	0.191 ± 0.012	94.3 ± 0.4	5.5 ± 0.4	2.1 ± 0.2	0.08
	41	0.234 ± 0.015	93.9 ± 0.4	5.9 ± 0.4	2.5 ± 0.2	0.11
	55	0.236 ± 0.015	93.7 ± 0.4	6.1 ± 0.4	2.7 ± 0.2	0.09
	69	0.309 ± 0.020	91.7 ± 0.5	8.0 ± 0.5	3.1 ± 0.3	0.11
	82	0.246 ± 0.016	93.5 ± 0.4	6.3 ± 0.4	3.3 ± 0.3	0.09
	96	0.250 ± 0.016	92.4 ± 0.5	7.4 ± 0.5	3.1 ± 0.3	0.12
	110	0.206 ± 0.013	92.5 ± 0.5	7.3 ± 0.5	2.6 ± 0.2	0.13 ± 0.05
	AVG	0.231 ± 0.015	93.1 ± 0.3	6.6 ± 0.3	2.77 ± 0.14	0.06 ± 0.03

#PU6	µm	Cr, wt%	Fe, wt%	Ni, wt%	Ir, ppm	Au, ppm
	14	0.331 ± 0.022	91.6 ± 0.5	8.1 ± 0.5	3.0 ± 0.3	0.12
	27	0.241 ± 0.016	92.3 ± 0.5	7.4 ± 0.5	2.9 ± 0.3	0.12
	41	0.186 ± 0.012	92.4 ± 0.5	7.4 ± 0.5	2.4 ± 0.2	0.11
	55	0.179 ± 0.012	90.9 ± 0.6	8.9 ± 0.6	2.9 ± 0.3	0.13
	69	0.193 ± 0.013	92.0 ± 0.5	7.8 ± 0.5	3.3 ± 0.3	0.13
	82	0.163 ± 0.011	92.3 ± 0.5	7.5 ± 0.5	2.3 ± 0.2	0.11
	96	0.148 ± 0.010	92.9 ± 0.4	6.9 ± 0.4	2.2 ± 0.2	0.10
	110	0.171 ± 0.011	93.5 ± 0.4	6.3 ± 0.4	3.0 ± 0.2	0.09
	123	0.155 ± 0.010	92.1 ± 0.5	7.8 ± 0.5	2.6 ± 0.2	0.12
	137	0.280 ± 0.018	93.0 ± 0.4	6.7 ± 0.4	2.7 ± 0.2	0.11
	AVG	0.205 ± 0.019	92.3 ± 0.2	7.5 ± 0.2	2.75 ± 0.11	0.04

Table EA4